Superficial Layers of the Medial Entorhinal Cortex Replay Independent of the Hippocampus

J. O'Neill[*], C.N. Boccara, F. Stella, P. Schoenenberger[†], J. Csicsvari[*]

IST Austria, Am Campus 1, A – 3400 Klosterneuburg, Austria

† Current Address: F. Hoffmann-La Roche Ltd, Roche Innovation Center Basel, Grenzacherstrasse 124, 4070 Basel, Switzerland

[*]Corresponding author. E-mail: jozsef.csicsvari@ist.ac.at, joneill@ist.ac.at

The hippocampus is thought to initiate systems-wide mnemonic processes through the reactivation of previously acquired spatial/episodic memory traces, which can recruit the entorhinal cortex as a first stage of memory redistribution to other brain areas. Hippocampal reactivation occurs during sharp wave/ripples, in which synchronous network firing encodes sequences of places. We investigated the coordination of this replay by recording assembly activity simultaneously in the CA1 region and superficial layers of the medial entorhinal cortex. We found that entorhinal cell assemblies can replay trajectories, independent of the hippocampus and sharp wave/ripples. This suggests that the hippocampus is not the sole initiator for spatial/episodic memory trace reactivation. Memory systems involved in these processes may include non-hierarchical, parallel components.

One Sentence Summary:

Medial entorhinal cortex can reactivate movement trajectories independent of the hippocampus during waking and sleep periods.

The hippocampus plays a principal role in the encoding, consolidation and recall of spatial/episodic memories(*1*, *2*), by forming cell assemblies that code for place and subsequently replaying their activity patterns(*3*, *4*). This replay, which represents discrete places or entire movement trajectories, can occur both in waking periods(*5*), while animals actively engage in a spatial task(*6–9*), and in periods of rest/sleep(*10*, *11*); each facilitating different stages of memory processing(*8*). In immobility/sleep periods, replay occurs in highly synchronized network activity during sharp wave/ripple (SWR) and is associated with memory consolidation(*8*, *12*, *13*). However, SWR-related replay during spatial memory tasks can predict the future behavioral choice of the animal and have been linked to memory recall(*8*, *9*). Because highly-synchronized hippocampal SWR activity recruits multiple brain areas(*14*), the prevailing view suggests that the hippocampus initiates replay during SWRs, and in doing so, is the primary coordinator for the consolidation of memory traces associated with place(*4*, *13*).

By contrast, the entorhinal cortex (EC) is thought to primarily assist the hippocampus in replay-associated mnemonic processing. During encoding, cells in the superficial layers of the medial EC (sMEC), particularly grid cells(*15*), provide the hippocampus with precise spatial coding through path integration(*16*). However, during SWR-associated replay, the EC is considered to act primarily as a relay, facilitating the transfer of replayed hippocampal memory traces to other cortical areas(*13*). However, at the sMEC and hippocampus may be able to act independently; sMEC cells may take part in replay independently of hippocampal SWR, initiating memory consolidation or recall. This latter scenario is in agreement with the hypothesis that memory trace reactivation can originate from multiple brain regions(*17*).

To test whether the sMEC replays waking experience, and to examine its relationship to hippocampal firing, we simultaneously recorded neurons from the CA1 region and sMEC (Fig. S1). Four rats were trained to perform a delayed non-match-to-sample spatial task on a continuous T-maze (Fig. 1A, see methods)(*18*). Before the task, rats foraged in a large arena to test the 2-dimensional spatial firing fields of our sMEC cells (Fig. 1B).

First, we characterized how sMEC neurons encoded space on the maze. Grid cell firing rates and spatial assembly patterns were better correlated between the open field and T-maze than non-grid cells (Fig. S3, 3A-C). This is in agreement with the tendency of grid cells to maintain similar firing fields in different environments(*19*). Nevertheless, the assemblies of sMEC neurons could represent unique locations on the maze, even when only considering grid cells(*20*); a Bayesian maximum likelihood method(*21*) accurately predicted the position of the animal on the track (reconstruction error; sMEC: 7.2 ± 0.6cm, n = 11 sessions. Grid cell only: 16.6433 ± 2.9cm, $\geq$ 10 cells: n = 4 sessions, mean $\pm$ SEM, Fig. S4).

EC cells can fire differentially at different phases of a spatial alternation task(*22*, *23*). To

test whether units showed task-related changes, we analyzed firing rates on runs to the choice point for the 4 possible trial phases (i.e., left sample, left choice, right sample and right choice); and asked if firing rates exhibited significant differences independent of head direction, speed and lateral position (see methods, Fig. S5A-C). CA1, grid and non-grid sMEC cells all showed significant rate modulation (Fig. S5F). Moreover, a similar proportion of cells exhibited significant rate changes on the return arms depending on trial type Fig. S5E,G). However, the firing fields were highly correlated across trial phases (Fig. S3D-E), indicating that task-related firing is expressed mainly through rate remapping(*24*). This indicates that both grid and non-grid sMEC populations exhibited mnemonic coding beyond path integration, that was linked to both trial type and the future trajectory of the animal.

Recent fMRI work in humans suggests that, similar to the hippocampus, the EC may reactivate imagined trajectories during recall(*25*). We looked for evidence of replay in the sMEC during transient periods of high network synchronization. Like the hippocampus, sMEC units showed transient increases in synchrony, during both waking and sleep/rest (high synchrony event: HSE, Fig. 2A-B, Fig. S6, see methods). To quantify whether such HSEs encoded maze trajectories, we subdivided each HSE into short windows (20ms, 10ms overlap) and used the Bayesian algorithm to identify the locations represented in each window. We then randomly rotated the linear place fields of cells within the event and asked whether the selected fit was better than that generated from the randomized place fields, for 95% of 1000 separate shuffles (Fig. 2B, Fig. S7, n = 11 sessions). Indeed, the distribution of the trajectory fit scores (replay score) were significantly different between the original and the place field randomized cases ($P<10^{-27}$ Kolmogorov-Smirnov test, KS, Fig 2D). Moreover the z-score of the original trajectory fits, normalized according to the shuffled distribution, were positive (Fig. S8). Similar results were obtained when we jittered spikes times instead of their place fields (Fig. S7,8). These significant replay events were detected throughout the maze, including during the delay, at both low and high speeds and often reflected locations remote from the animal (Fig. S9). It is unlikely that these replay events occurred as a result of theta phase precession since they formed a mix of forward and reverse replay and had a slope that was 2-3 fold higher than that expected from phase precession (Fig. S10-11).

Waking sMEC replay during the task may follow hippocampal SWR replay or alternatively operate independently. We checked whether spiking in the CA1 encoded trajectories that were coherent with sMEC sequences. We used the Bayesian decoding procedure to establish the places represented in the CA1 during sMEC events. Having established the trajectory encoded by the sMEC sequence, we generated a replay coherence score to quantify fit of the sMEC trajectory to the encoded CA1 places (Fig. 2C). This score was compared to that generated following the shuffling of CA1 spike times within the event (see methods). Surprisingly, sMEC

replay events were not accompanied by coherent CA1 activity: (the distribution of the coherence scores was similar to that of the shuffled scores (all p>0.6, KS test n = 8 sessions, Fig 2F, Fig. S12A-B). Moreover, the shuffled distribution-normalized z-score of the coherence values were not above zero more often than chance (Fig. S13A-B, p>0.3 binomial test). We also detected significant replay events in the CA1 (Fig. 2E, Fig. S14) and sMEC activity was not related to CA1 replay (p>0.18, KS test, Fig. 2G, Fig. S12 A,B, but in z-scores: place field rotation sequences at low speed p=0.01795, all other p>0.14, Fig S13 A-B). The lack of coherent activity was not due to the sparse firing within the other region: even one cell alone showed coherent activity with the remaining cells within the same region during replay, and coherence improves when 2 or 3 cells are tested with the rest (Fig. S13 C,D). Trajectories that encoded the current location of the animal within theta oscillatory cycles in a region always exhibited significantly stronger coherence with activity in the other region than during trajectory replay (p<10^{-15}, Anova, , Fig. S15). Performing a time-shifted coherence analysis did not significantly change the coherence values indicating that synaptic delay was not a cause of the lack of coherent trajectory replay (Fig S16).

Significant CA1 and sMEC replay events were not correlated in time (Fig. 2I). Moreover, sMEC replay was not associated with an increase in ripple power or SWRs, while CA1 replay events at low speeds were (Fig. 2H,I). This shows that sMEC can encode task-related mnemonic sequences independently from the hippocampus, suggesting an independent role for the sMEC in encoding/recall related to memory sequences.

Our coherence analysis examined whether trajectory replay in one region aligned with places expressed in the other region. However, nonaligned trajectory segments could still overlap with places expressed in the other region. Therefore, we randomly selected places from other trajectory replay events and found that these randomized places exhibited weaker coherence scores than the original ones (Fig. S17A-B, all p<0.05 KS test). A possible explanation for this findings is that many of these replayed trajectories originate from the current location of the animal; hence place-related firing in one region overlapped with the replayed trajectory in the other.

Entorhinal replay during active waking periods appeared to predominantly operate independently of hippocampal reactivation. Next we tested whether sMEC cells can replay trajectories independently from the hippocampus during rest/sleep epochs or whether these were driven by CA1 firing, similar to the deep medial EC layers, which are directly innervated by CA1 place cells (*26*). We first asked whether sMEC sequences could be detected during rest, and then examined their relationship to hippocampal network activity (Fig. 3A-C). Similar to waking epochs, HSEs during rest exhibited significant sMEC replay (Fig. 3E, Fig. S7, all P<10^{-27} KS test, see also Fig. S8). The replay coherence analysis showed that sMEC replay events were not accompanied by related CA1 spatial firing (all P>0.1, KS test, Fig. 3F, Fig. S12C,13). We then

examined the degree to which CA1 replay influences the activity of sMEC cells (Fig. 3D,E, Fig. S14). In this case sMEC assembly activity exhibited coherence with CA1 replay, when sequences were detected using the spike jittered shuffling (p<0.038 KS test, Fig. S12C), but not with place field rotation (p>0.07, KS test, Fig. 3F). Given that hippocampal SWR-associated replay engage the majority of the dorsal hippocampus(*9, 27*), we examined the relationship of sMEC replay with SWRs. CA1 ripple power only showed a marginal increase during sMEC replay compared to CA1 replay, even for sMEC events exhibiting coherent replay with CA1 (Fig. 3G). Indeed, out of 202 events, only 5.9% of sMEC replay events were temporally aligned to detected SWR (peak of HSE ± 25 ms from the peak of the SWR), in contrast to 29.9% (184/674) for CA1 replay (Fig. 3H). HSEs in the two regions were also independent; only 4.4% of sMEC replay events occurred within 25ms of CA1 HSEs, whether or not we could detect replay there (Fig. 3H). However, CA1 activity expressed places that, higher than chance, overlapped with nonaligned parts of the sMEC trajectories, and vice versa. Therefore, even in rest the two regions could weakly interact during reactivation (Fig. S17C-D, all p<0.01, KS test).

Our data showed that sMEC cells including grid cells fired in relation to the memory task on the maze. Furthermore, sMEC was involved in the mnemonic trajectory sequence coding: we saw that the sMEC produces bursts of activity, during both waking and sleep/rest that contained sequences reflecting task-related trajectories on the maze. Such events tended to occur independently from hippocampal trajectory replay and associated SWRs. Moreover, trajectory replay that occurred in the sMEC was not associated with temporally-aligned coherent activity in CA1. This suggests that the sMEC can trigger its own replay events and initiate recall and consolidation processes independent of hippocampal SWRs, whereas deep EC layers are directly influenced by CA1 replay(*26*). However, some weak coordination may exist between CA1 and sMEC and in some instances replayed trajectories contain locations that were expressed in the other region.

Overall, these findings indicate that the EC can act independently in mnemonic processes rather than having a subservient role to the hippocampus. Therefore, the hippocampus and EC may be considered as interrelated but parallel systems in initiating reactivation and they may recruit different brain pathways and may have different roles.

References and notes

1. J. O'Keefe, L. Nadel, *The Hippocampus as a Cognitive Map* (Oxford University Press, 1978).

2. G. Riedel *et al.*, Reversible neural inactivation reveals hippocampal participation in several memory processes. *Nat.Neurosci.* **2**, 898–905 (1999).

3. G. Buzsaki, Two-stage model of memory trace formation: a role for "noisy" brain states. *Neuroscience.* **31**, 551–570 (1989).

4. J. L. McClelland, B. L. McNaughton, R. C. O'Reilly, Why there are complementary learning systems in the hippocampus and neocortex: insights from the successes and failures of connectionist models of learning and memory. *Psychol.Rev.* **102**, 419–457 (1995).

5. J. O'Neill, T. Senior, J. Csicsvari, Place-selective firing of CA1 pyramidal cells during sharp wave/ripple network patterns in exploratory behavior. *Neuron.* **49**, 143–155 (2006).

6. S. P. Jadhav, C. Kemere, P. W. German, L. M. Frank, Awake Hippocampal Sharp-Wave Ripples Support Spatial Memory. *Science.* **336**, 1454–1458 (2012).

7. D. J. Foster, M. A. Wilson, Reverse replay of behavioural sequences in hippocampal place cells during the awake state. *Nature.* **440**, 680–683 (2006).

8. D. K. Roumis, L. M. Frank, Hippocampal sharp-wave ripples in waking and sleeping states. *Curr. Opin. Neurobiol.* **35**, 6–12 (2015).

9. B. E. Pfeiffer, D. J. Foster, Hippocampal place-cell sequences depict future paths to remembered goals. *Nature.* **497**, 74–79 (2013).

10. A. K. Lee, M. A. Wilson, Memory of sequential experience in the hippocampus during slow wave sleep. *Neuron.* **36**, 1183–1194 (2002).

11. M. A. Wilson, B. L. McNaughton, Reactivation of hippocampal ensemble memories during sleep. *Science.* **265**, 676–679 (1994).

12. G. Girardeau, K. Benchenane, S. I. Wiener, G. Buzsaki, M. B. Zugaro, Selective suppression of hippocampal ripples impairs spatial memory. *Nat.Neurosci.* **12**, 1222–1223 (2009).

13. G. Buzsaki, The hippocampo-neocortical dialogue. *Cereb.Cortex.* **6**, 81–92 (1996).

14. N. K. Logothetis *et al.*, Hippocampal–cortical interaction during periods of subcortical silence. *Nature.* **491**, 547–553 (2012).

15. T. Hafting, M. Fyhn, S. Molden, M. B. Moser, E. I. Moser, Microstructure of a spatial map in the entorhinal cortex. *Nature.* **436**, 801–806 (2005).

16. B. L. McNaughton, F. P. Battaglia, O. Jensen, E. I. Moser, M. B. Moser, Path integration and the neural basis of the "cognitive map." *Nat.Rev.Neurosci.* **7**, 663–678 (2006).

17. G. R. Sutherland, B. McNaughton, Memory trace reactivation in hippocampal and neocortical neuronal ensembles. *Curr.Opin.Neurobiol.* **10**, 180–186 (2000).

18. R. M. J. Deacon, J. N. P. Rawlins, T-maze alternation in the rodent. *Nat. Protoc.* **1**, 7–12 (2006).

19. E. I. Moser *et al.*, Grid cells and cortical representation. *Nat. Rev. Neurosci.* **15**, 466–481 (2014).

20. K. Gupta, L. A. Keller, M. E. Hasselmo, Reduced spiking in entorhinal cortex during the delay period of a cued spatial response task. *Learn. Mem. Cold Spring Harb. N.* **19**, 219–230 (2012).

21. K. Zhang, I. Ginzburg, B. L. McNaughton, T. J. Sejnowski, Interpreting neuronal population activity by reconstruction: unified framework with application to hippocampal place cells. *J. Neurophysiol.* **79**, 1017–1044 (1998).

22. L. M. Frank, E. N. Brown, M. Wilson, Trajectory encoding in the hippocampus and entorhinal cortex. *Neuron.* **27**, 169–178 (2000).

23. P. A. Lipton, J. A. White, H. Eichenbaum, Disambiguation of overlapping experiences by neurons in the medial entorhinal cortex. *J. Neurosci. Off. J. Soc. Neurosci.* **27**, 5787–5795 (2007).

24. S. Leutgeb *et al.*, Independent codes for spatial and episodic memory in hippocampal neuronal ensembles. *Science.* **309**, 619–623 (2005).

25. A. J. Horner, J. A. Bisby, E. Zotow, D. Bush, N. Burgess, Grid-like Processing of Imagined Navigation. *Curr. Biol. CB.* **26**, 842–847 (2016).

26. H. F. Ólafsdóttir, F. Carpenter, C. Barry, Coordinated grid and place cell replay during rest. *Nat. Neurosci.* (2016), doi:10.1038/nn.4291.

27. A. Ylinen *et al.*, Sharp wave-associated high-frequency oscillation (200 Hz) in the intact hippocampus: network and intracellular mechanisms. *J.Neurosci.* **15**, 30–46 (1995).

28. J. Csicsvari, H. Hirase, A. Czurko, A. Mamiya, G. Buzsaki, Oscillatory coupling of hippocampal pyramidal cells and interneurons in the behaving Rat. *J.Neurosci.* **19**, 274–287 (1999).

29. K. D. Harris, H. Hirase, X. Leinekugel, D. A. Henze, G. Buzsaki, Temporal interaction between single spikes and complex spike bursts in hippocampal pyramidal cells. *Neuron.* **32**, 141–149 (2001).

30. T. Stensola, H. Stensola, M.-B. Moser, E. I. Moser, Shearing-induced asymmetry in entorhinal grid cells. *Nature.* **518**, 207–212 (2015).

31. R. F. Langston *et al.*, Development of the Spatial Representation System in the Rat. *Science.* **328**, 1576–1580 (2010).

32. J. O'Neill, T. J. Senior, K. Allen, J. R. Huxter, J. Csicsvari, Reactivation of experience-dependent cell assembly patterns in the hippocampus. *Nat. Neurosci.* **11**, 209–215 (2008).

33. J. H. Zar, *Biostatistical analysis* (Prentice Hall, Upper Saddle River, N.J, 4th ed., 1999).

34. T. J. Davidson, F. Kloosterman, M. A. Wilson, Hippocampal Replay of Extended Experience. *Neuron.* **63**, 497–507 (2009).

35. A. D. Grosmark, G. Buzsáki, Diversity in neural firing dynamics supports both rigid and learned hippocampal sequences. *Science.* **351**, 1440–1443 (2016).

36. R. U. Muller, J. L. Kubie, The firing of hippocampal place cells predicts the future position of

freely moving rats. *J. Neurosci.* **9**, 4101–4110 (1989).

37. W. E. Skaggs, B. L. McNaughton, M. A. Wilson, C. A. Barnes, Theta phase precession in hippocampal neuronal populations and the compression of temporal sequences. *Hippocampus*. **6**, 149–172 (1996).

38. T. Hafting, M. Fyhn, T. Bonnevie, M.-B. Moser, E. I. Moser, Hippocampus-independent phase precession in entorhinal grid cells. *Nature*. **453**, 1248–1252 (2008).

Acknowledgments:

Fig. 1. sMEC and CA1 firing patterns on the T-maze.

A) Behavioral paradigm. Animals first explored a large arena, then slept in a sleep box. Next the animal performed >30 trials of a non-match-to-sample task on a modified T-maze, followed by a second sleep session. The blue arrow marks the choice point, circle the goal location and blue-highlighted region marks the central arm.

B) Spatial firing patterns of simultaneously recorded sMEC putative excitatory units (17/27 displayed, red) and a representative CA1 pyramidal cell (1/53 black, bottom right). The position of spikes emitted (red dots) and path of the animal (grey) are shown as well as the smoothed rate maps. The peak firing rate of each cell (Hz) is shown above the place-rate maps.

C) Linear rate maps of all 27 sMEC excitatory units, ordered by the location of their peak firing rate on the right choice trial.

Fig. 2. sMEC replay during exploration

A) Local field potential centered on a sMEC HSE (highlighted purple, peak: dotted grey line). Channels were taken from different tetrodes (black: CA1, red: sMEC). Raster plot: unit activity sorted by location of their peak firing rate on left choice trials (black: CA1, red: sMEC, blue: interneurons).

B) Position reconstruction during the sMEC HSE shown in (A). Left: linearized sMEC rate maps, sorted by the same order as the raster plot. Middle panels: position reconstruction in MEC using maps for the 4 trial conditions (red line: line of best fit with the highest replay score). Black shading represents the location with the highest probability, within each window. Right panel: Position of the animal (yellow dot) and reconstructed trajectory (red), overlaid on tracking data from the task (grey).

C) Examples of sMEC (highlighted red) and CA1 position reconstruction using maps of trial conditions with the best fit, during sMEC HSEs. Each red line of best fit was generated from sMEC data.

D,E) The cumulative distribution of replay scores for HSEs detected in the sMEC (D, red) and CA1 (E, black). Shuffled distributions are shown in cyan. Top: HSE's during pauses in exploration, bottom: during movement. ** $P<10^{-27}$ KS test

F,G) The cumulative distribution of replay coherence scores between sMEC repay andCA1 activity (F, red) and CA1 replay with sMEC (G, black). Shuffled distributions are shown in cyan. All $P >0.18$, KS test. Layout as in F&G.

H) Normalized CA1 ripple power during replay. sMEC: red, CA1: black

I) Cross correlation of event times between CA1 (black) and sMEC (red) significant replay and SWR, and between sMEC significant replay and all CA1 HSEs (blue).

Blue arrow marks the choice point, circle the goal location. Error bars: SEM.

Fig. 3. Independent sMEC and CA1 replay during rest in the sleep box

A) Local field potential centered on a sMEC HSE (highlighted purple, peak: dotted line), detected during a rest session. Channels were taken from different tetrodes (black: CA1, red: sMEC). Raster plot: unit activity sorted by location of their peak firing rate on right choice trials (black: CA1, red: sMEC, blue: interneurons).

B) Linearized rate maps for CA1 (black) and sMEC (red) excitatory units, sorted as in (A).

C,D) Examples of detected significant sMEC (C) and CA1 region (D) replay, with the corresponding position reconstruction in the other brain region using maps of trial conditions with the best fit. The left panel in (C) shows the position reconstruction for the sMEC HSE in (A).

E) The cumulative distribution of replay scores for HSEs detected in sMEC (top panel) and CA1 (bottom panel). Shuffled distribution shown in cyan. ** $P<10^{-44}$ KS test.

F) The cumulative distribution of coherence for sMEC repay withCA1 activity (top, red) and CA1 replay to sMEC (bottom, black). None of original and shuffled score distributions are significantly different. Shuffled distributions shown in cyan. sMEC-CA1 P>0.1, CA1-sMEC P>0.07, KS test.

G) Normalized CA1 ripple power during replay. sMEC: red, CA1:black

H) Cross correlation of event times between CA1 (black) and sMEC (red) significant replay and SWR, and between sMEC significant replay and all CA1 HSEs (blue).
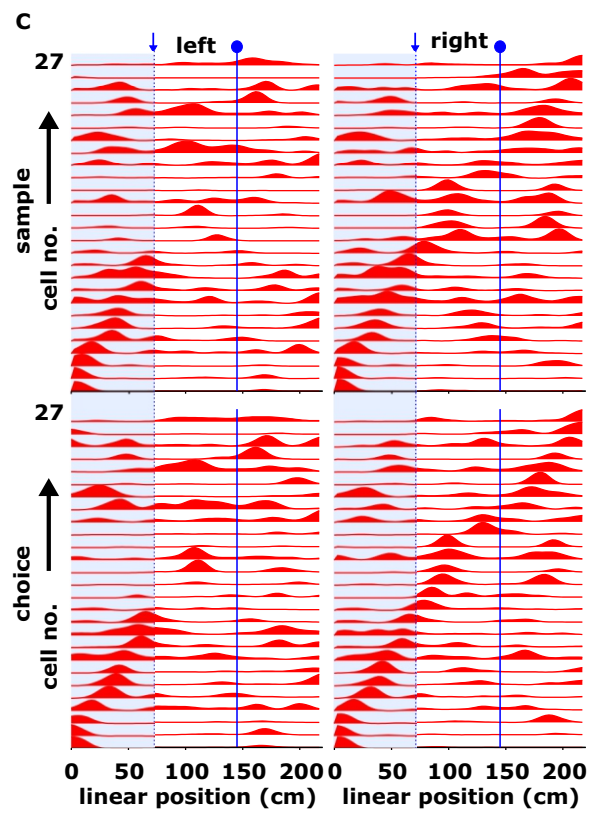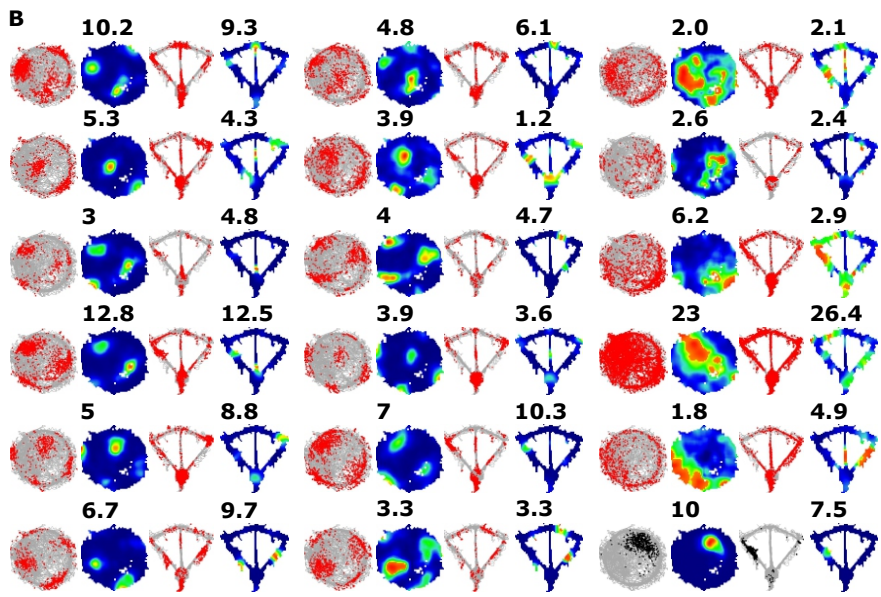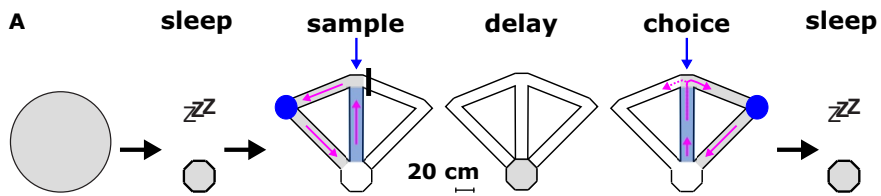
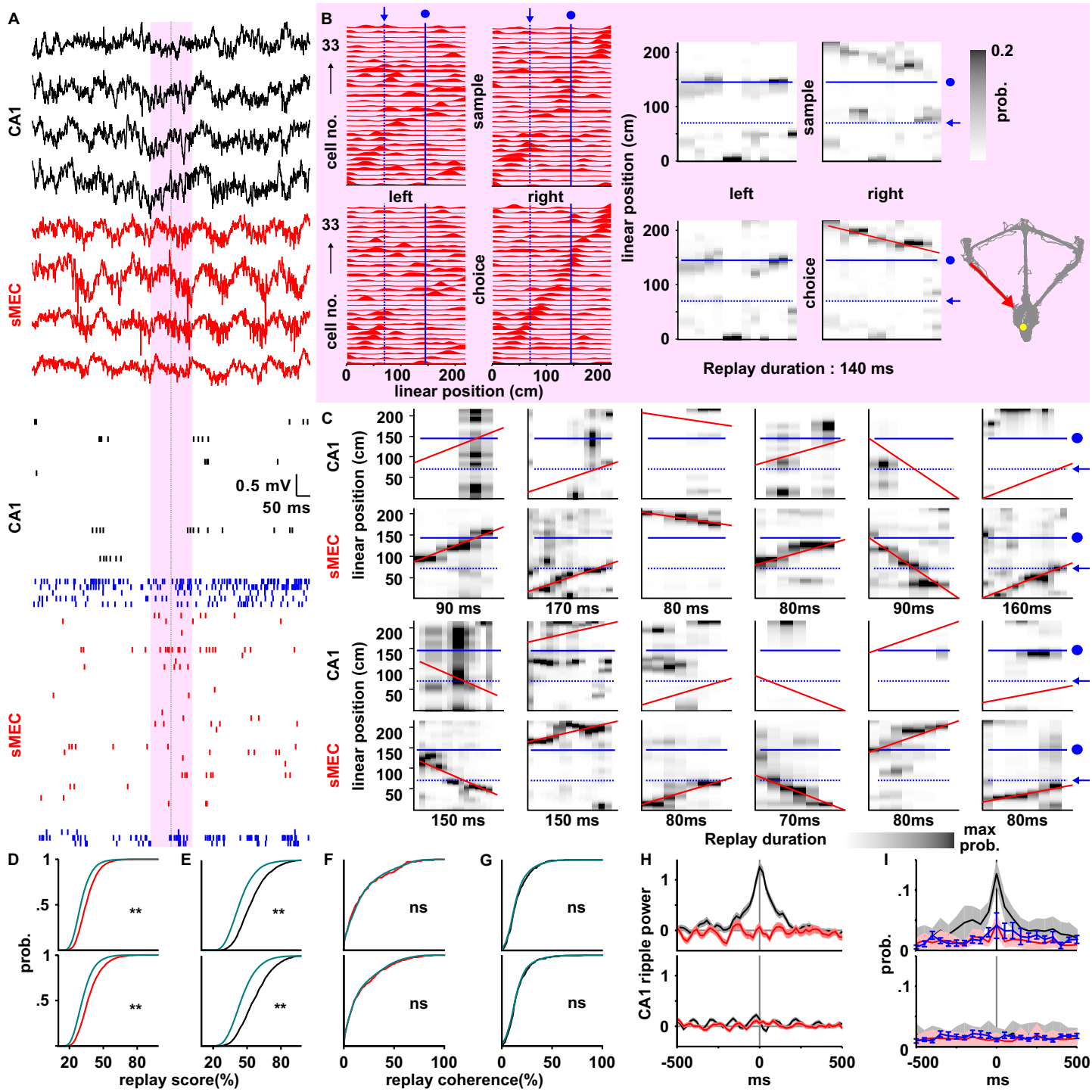Blue arrow marks the choice point, circle the goal location. Error bars: SEM.

Supplementary Materials:

Materials and Methods

Figures S1-S17

References (*28-38*)

A

sleep → sample → delay → choice → sleep

20 cm

B

10.2 9.3 4.8 6.1 2.0 2.1
5.3 4.3 3.9 1.2 2.6 2.4
3 4.8 4 4.7 6.2 2.9
12.8 12.5 3.9 3.6 23 26.4
5 8.8 7 10.3 1.8 4.9
6.7 9.7 3.3 3.3 10 7.5

C

27 left right

sample cell no.

27 choice cell no.

linear position (cm) linear position (cm)
0 50 100 150 200 0 50 100 150 200

A

CA1

sMEC

CA1

0.5 mV
50 ms

sMEC

B

33 ↑ cell no.

sample

left   right

33 ↑ cell no.

choice

left   right

linear position (cm)

linear position (cm)

0.2 prob.

sample

left   right

choice

left   right

Replay duration : 140 ms

C

CA1 linear position (cm)

sMEC linear position (cm)

90 ms   170 ms   80 ms   80 ms   90 ms   160ms

CA1 linear position (cm)

sMEC linear position (cm)

150 ms   150 ms   80ms   70ms   80ms   80ms

Replay duration

max prob.

D   **E**   **F**   **G**

prob.

1   1

.5   **   .5   **   ns   ns

1   1

.5   **   .5   **   ns   ns

20 50 80   20 50 80   0   50 100   0   50 100
replay score(%)   replay coherence(%)

H

CA1 ripple power

1

0

0

-500   0   500
ms

I

prob.

.1

0

.1

0

-500   0   500
ms

Supplementary Materials for

Superficial Layers of the Medial Entorhinal Cortex Replay Independent of the Hippocampus

J. O'Neill[*], C.N. Boccara, F. Stella, P. Schoenenberger[†], J. Csicsvari[*]

.

[*]correspondence to: jozsef.csicsvari@ist.ac.at, joneill@ist.ac.at

This PDF file includes:

Materials and Methods
Figs. S1 to S17

Materials and Methods

<u>Surgery</u>

Four male rats (300–400 g) were implanted with 16 independently movable wire tetrodes under deep anesthesia using isoflurane (0.5%–3%), oxygen (1–2 l/min), and an initial dose of buprenorphine (0.1 mg/kg). Our electrodes were arranged in two bundles: one targeting CA1 and the other to target the superficial layers (II/III) of the medial entorhinal cortex (sMEC). The electrodes were constructed from four 17 um or 8 individual 12 um tungsten wires respectively, twisted and then heated in order to bind them into a single bundle. The tips were then gold plated to reduce their electrode impedance to 200–600 kΩ. During surgery, two craniotomies were centered above the CA1 and the medial EC (MEC). The electrodes were then implanted at a 6-10 degree angle, relative to the skull. In 3 animals the sMEC bundle consisted of 4 rows (anterior-posterior axis) of 2 tetrodes, covering a total area of .4 mm (medial-lateral axis, ML) by 1.2mm (anterior-posterior, AP), i.e. 400 μm separation. These electrodes were then implanted into a region between -4.0 and -4.4 ML and -7.6 and -8.8 mm AP, relative to bregma. In a further rat, the electrodes were arranged (from anterior to posterior) in a row of two electrodes, followed by a row of 3 electrodes and finally by a row of two, the most lateral of which consisted of an 8-wire octrode. In this case the electrodes were implanted within a region -3.8 and -4.6 ML and -8 and -8.8 mm AP, relative to bregma. The bundles targeting the CA1 (centered on -2.5 ML,-3.6 AP) were implanted into the deep layers of the neocortex. The electrodes targeting the MEC were 1-2.5mm longer, and implanted into the deep layers (V/VI) of the MEC. Two screws positioned above the cerebellum served as ground and reference electrodes. Six additional stainless-steel anchor screws were used in order to permanently attach the microdrive assembly to the scull. The paraffin wax-coated electrodes and the microdrive apparatus were then daubed with dental acrylic to encase the electrode-microdrive assembly and anchor it to the screws in the skull. Following a recovery period of 7 days, the tetrodes were lowered in 50–200 μm steps each day into the CA1 region and superficial layers of the MEC, over a further period of up to 7–14 days (see training procedures below). Two 32-channel unity-gain preamplifier panels were used to reduce cable-movement artefacts. Wide-band (0.4 Hz to 9 kHz) recordings were taken, and the amplified local field potential and multiple-unit activity were continuously digitized at 24 kHz. All procedures involving experimental animals were carried out in accordance with Austrian (Austrian federal Law for experiments with live animals) animal law under a project license approved by the Austrian Federal Science Ministry.

<u>Apparatus</u> <u>and</u> <u>training</u> <u>procedures</u>

The animals were housed in a separate room and were taken to the recording room each day prior to the experiments. Following the recovery period (7 days), the animal was exposed to both a large open field arena and T-maze apparatus, over a period of 14 days. The open field arena consisted of either a circular environment (radius 1.2 m), or a large rectangular arena (1.5m x 2m). The T-maze comprised a central arm and two return arms, containing a total of 220cm of linear track for both left and right turns. The animal was placed on food restriction (>85 % of initial weight with a 10 gram gain each week), once it had passed the 7 day recovery period and exceeded their pre-surgery weight. Each animal was then trained for pellet chasing in an open field environment and to collect rewards on the T-maze. From this point, the animal experienced the same daily

procedure until the cessation of the experiment, which was as follows. At the beginning of each day electrodes were lowered. Following a break of 1 to 2 hours, the animal was then recorded in the rest box (see description of T-maze below), then placed in the open field, and then again in the rest box. Next the animal was placed on the T-maze, for training or recording. After the last trial, the animal remained in the rest box, for post task rest/sleep. The final rest session was omitted in one rat (3 sessions out of 12 recording days).   Two bundles of light emitting diodes mounted either side of the headstage were used to track the location and head direction of the animal, and the position/head direction of the animal sampled at 50 Hz.

T-maze delayed non-match-to-sample task.

The T-maze apparatus consisted of an octagonal rest box, from which the animal could travel directly to the central arm and return through two addition arms to the right and left (see Fig.1a). This rest box contained 80 cm high pneumatically controlled doors, which were used to control the animals exit onto the central arm at the beginning of each trial sample and choice phase, or access from the return arms, on completion. A single trial would first contain a sample phase, in which a door would be raised to prevent the animal from choosing one side of the maze. When the animal reached the goal (placed at the far corner of the maze, see Fig. 1a), a pellet would be dropped from an overhead pellet feeder. Following this, the door would be raised on the rest box to allow the animal to return. Once inside the rest area, the animal would receive another food pellet, and remain for a further 20-30 seconds, before lowering the door blocking the central arm, to provide a free choice of the left or right arms. The animal would be rewarded with a pellet if it selected the opposite arm to that baited on the sample trial. Regardless of whether the correct arm was selected, the door on the rest area would then be lowered, to allow the animal to return to the rest area, and subsequently begin a new trial.   The sample trials were pseudo-randomly organized so that the animal would be forced to go either left or right, with no more than 3 consecutive trials for either side. In this way, a single traversal of the T-maze could be one of 4 trial phases: sample left or right and choice left or right. Behavioral shaping for this task began by first training the animal to collect a pellet from the goal and return to the rest area. This was performed by training blocks of 6 trials of sample trials for one side followed by another block of 6 for the alternate side to prevent the animal developing a preference to one arm. Once the animal's behavior had been shaped with this procedure, the animal was exposed to 10 trials of rewarded alternation, without a delay in the rest area. On the next day, the animal was exposed to 20 trials, this time with a 10 second delay. This procedure was then repeated with a 20-30 second delay on the following day, which continued for a further day, if the animal had not yet reached a performance level of 70% correct trials. In this way the animal could perform the task with shaped behavior, without over training. All animals achieved greater than 75% accuracy on each recording day (mean: 82.7%, n = 12 sessions, minimum 36 trials).

Data Analysis

Spike sorting

The spike detection in the local field potential and sorting was performed as previously described(*28*). Action potentials were extracted by first computing power in the 800-9000 Hz range within a in a sliding window (12.8 ms). Action potentials with a

power of >5 SD from the baseline mean were selected and spike features were then extracted by using principal components analyses. The detected action potentials were then segregated into putative multiple single units by using automatic clustering software(*29*) (http://klustakwik.sourceforge.net/). These clusters were then manually refined by a graphical cluster cutting program(*28*). Only units with clear refractory periods in their autocorrelation and well-defined cluster boundaries were used for further analysis. We further confirmed the quality of cluster separation by calculating the Mahalanobis distance(*29*) between each pair of clusters. Periods of waking spatial exploration, immobility, and sleep were clustered together and the stability of the isolated clusters was examined by visual inspection of the extracted features of the clusters over time. Pyramidal cells and interneurons in the CA1 region were discriminated by their autocorrelations, firing rate, and wave forms, as previously described(*28*). Putative MEC excitatory cells were identified by their firing rate. In this way we were able to identify the activity of 295 putative excitatory MEC neurons, including 91 grid cells, as well as 410 CA1 pyramidal units.

Generation of rate maps

Two-dimensional place-rate maps in the open field and T-maze were calculated using the following procedure. First, the environment was subdivided into a grid, containing 2x2cm bins. A 2x2cm square was overlaid on this grid, for each spike of a given cell, centered on the position of the animal when the spike was emitted. Each bin was then incremented by the degree to which this square overlapped with it. The same procedure was then performed with the tracking data to produce a map of occupancy. Occupancy and spike matrices were then smoothed with a Gaussian kernel (SD = 3 bins), and divided to produce a place-rate maps. To test for rate modulation of trial type and reconstruction of replayed trajectories, we transformed the T-maze into a linear track. We generated a line down the center of each section of the track totaling 220 cm for left and right turns. Linear position was calculated by detecting the closest point to the closest straight line segment, for each tracking sample. Runs were segregated into left sample, left choice, right sample and right choice. For the Bayesian reconstruction analysis, the linearized animal position was subdivided into 75 bins. Spike counts and occupancy in these bins were smoothed with a Gaussian kernel (SD: 2 bins) and divided to produce linear rate maps. For waking replay analysis time windows containing high synchrony windows (HSE's, described below) were removed from the data, prior to calculation of the linear rate maps.

Grid score

To identify grid cells among the set of cells recorded from MEC we first fitted an ellipse to the centres of the six innermost detected fields of the autocorrelogram (*30*). From this fit we obtained the ellipticity value (the ratio between the major and minor axis size) and the orientation of the major axis. We then computed the geometrical transformation necessary to morph this ellipse into a perfect circle (a compression along the major axis of a magnitude equivalent to the ellipticity score) and we applied it to the (x,y) value matrix of the autocorrelogram. The result of this operation, in the presence of an elongated grid, is to put the 6 peaks at the same distance from the centre, thus obtaining a regular hexagon on which to calculate the grid score. This was calculated using a measure similar to the one previously described in (*31*). For each cell the grid score was computed for the original autocorrelogram and then compared to a null

4

distribution of scores similarly computed on the autocorrelograms obtained from 100 shuffling of the cell spike times. For each shuffle we generated a new firing rate map from data in which the cell's spike train had been randomly permuted relative to the position of the animal by at least 30 s (*26*). A cell was labelled as a grid cell if its grid score exceeded the 95th percentile of the associated null distribution. With this procedure we identified 91 grid cells.

Coherence and Sparsity

Coherence(*32*) and sparsity(*33*) provide measures of rate map spatial selectivity. Coherence reflects the similarity of the firing rate in neighboring bins, and is the Fisher z–transform of the correlation between the rate in a bin and the average rate of its eight nearest neighbors. Sparsity represents the proportion of the environment in which a cell fires, corrected for dwell time, and is defined as $(\Sigma P_i R_i)^2 / \Sigma P_i R_i^{\,2}$, where P_i is the probability of the rat occupying bin i, R_i is the firing rate in bin i.

Assembly similarity score

We were interested in comparing spatial representations between environments of different geometries (i.e. T-maze vs. open field). We thus used a method to compare spatial overlap between pairs of cells in different environments/conditions, as previously described(*32*). In a given session, we calculated a pixel-by-pixel correlation between rate maps for each pair of cells, providing a matrix representing the similarity of place fields within a population of cells. Correlating matrices produced from two sessions provided an indication of the similarity of spatial representation between them, independent of differences in the geometry of the environment or even any global rotational translations of the rate maps. Matrices across all sessions for a given session type were concatenated, and a single correlation performed between the data from the two session types (e.g. open field vs. T-maze) to give an assembly similarity score (error bars: 95% CI of the correlation coefficient)(*33*). For consistency, the same method was used to compare similarity of spatial representation across different trial phases on the T-maze.

Ancova analysis

The ancova analysis was performed using rates established on the first 64 cm of the start track and last 64 cm of the return arm, which represented regions of the maze with the most stereotyped behavior. These sections were divided into 8 spatial bins along the path, in which rate, mean lateral position, head direction and speed were calculated on each trial. Head direction was linearized using the following procedure. First the mean head direction was established across the whole session, on the section of the track being analyzed. Tracking samples with a head direction that exceeded ± 90 degrees from this mean were excluded from further analysis, leaving a potential 180 degrees, which was transformed into 20 bins. Lateral position was calculated as the deviation from the center of the track. We calculated an average speed, lateral position and head direction in each bin, as well as rate, for each trial. Only units that fired >50 spikes within the section of the track in question were included for further analysis. Firing rates were considered separately for the left and the right returns arms when the return arm portions were analyzed. On the central arm: n = 150 CA1, n = 88 grid and n = 109 non-grid cells fired sufficient number of action potentials to perform the analysis whereas, on the return arms n = 273 CA1, n = 175 grid, n = 197 non-grid cells met the same criteria. We then used an ancova (using R software package) in order to ask if rate varied with trial phase (factors:

sample/choice and additional factor of left/right when the central arm), given changes in the behavioral variables.

Bayesian reconstruction of position

We used Bayesian place prediction(*21*) to first establish whether our population of sMEC units would provide sufficient spatial information to reconstruct position during exploration. We established population vectors in 500 ms windows (250 ms overlap, each containing at least 1 spike) while the animal was engaged in the T-maze task (excluding delay periods). The linear rate maps established over the whole task provide a firing probability for each spatial bin. The formula below gave the probability that a given population vector represented a given place:

$$P(x|\mathbf{n}) = P(\mathbf{n}|x)P(x)/P(\mathbf{n}).$$

P(x) represent the probability that the animal is at a given location considering the exploration session was set to a uniform distribution not to bias our analysis by any place preference of the animal(*21*). P(n|x) represents the conditional probability that a given spike count occurs at a location. This was estimated using the firing rates of the place-rate maps, assuming that the number of spikes follow a Poisson distribution. P(n), the normalizing constant, was used to ensure that P(x|n) summed up to 1. The location with the maximum probability was selected as the reconstructed position. In order to test the success of this prediction we used a cross-validation approach, by reconstructing the positions using maps established on all trials except the trial being currently decoded. Error measurements represented the absolute distance between the middle of the reconstructed bin to the real position of the animal. One recording session contained less than 15 sMEC units, and was excluded for further decoding analysis.

High Synchrony Events (HSE)

High synchrony periods were detected using the multi-unit activity of clustered spikes, similar to that previously described(*34*). We selected the clustered spikes from units designated as excitatory cells and segregated them according to where they were recorded (i.e., sMEC or CA1). These two groups were then analyzed separately to calculate the times of HSE's in each region. The combined activity of excitatory cells was binned into 1 ms bins and smoothed with a Gaussian kernel (SD = 15 ms), to produce a curve representing the synchronous spiking rate over time. HSE detection began when this curve passed 3 SD above the mean. The envelope of the HSE was extended until the curve again reached the mean rate, either side of this crossing. The peak of the HSE represented the peak of the curve within this envelope. Events containing fewer than 5 spikes, 4 cells or with less than 10% of the population of neurons active were rejected, as were events shorter than 75ms or greater than 750 ms. The beginning of the HSE was then adjusted to the time of the first spike. The HSE was then subdivided into 20ms windows, with a 10 ms overlap, until the last window containing a spike was reached. Following this procedure, all events with less than 5 windows were rejected from further analysis.

Replay during HSE's

HSE detection produced candidate events from which to detect replay. Within each event, we generated a series of population vectors within time windows defined by the

HSE detection. Using the same Bayesian analysis described above and linear rate maps established from each trial type we reconstructed probability density functions over position, for each time window in the event containing spikes. We used the method previously described (*34*) to establish a linear fit through each reconstruction (representing a putative linear trajectory through the environment), as well as a score representing the quality of this fit. Briefly, we iteratively generated a series of all possible linear trajectories through the environment. For each potential trajectory, we summed the probabilities from 4 position bins closest to the line, on both sides, to allow for trajectories with local variations in velocity. Locations were wrapped at the end of the track. We then tallied these sums across all time windows. This sum was normalized by the number of windows and expressed as a percentage, giving a replay score that provided a measure of the density of probability along a given trajectory. From this fit we could extract the start and end location of the replay, as well as its velocity. This was repeatedly performed across all possible trajectories in order to find the most likely replayed trajectory for a given trial phase. Such reconstructed trajectories may reflect a single location. We therefore first removed trajectories that either covered less than 4 position bins (11.73 cm) or had a fitted trajectory with an absolute slope of less than 200 cm/s from further analysis, un less indicated in the text (Fig. S11). The fit with the highest score across all trial phases (sample left/right and choice left/right) was selected as the replayed linear trajectory. We compared such a fit against shuffled data to generate a significance value, through the following procedure. First, for each cell, the linear place fields constructed from the same trial type were randomly shifted along the track independently, with bins extending off the end of the track wrapped to the start. Next, we established replay scores from the shuffled data, over 1000 different shuffles. This method preserved spike timing and firing rate statistics while disrupting the spatial coding of the units used in the reconstruction. In order to test whether the sequences required assembly activity to follow a precise temporal order we employed a 'spike jitter' shuffling method. For this method the spike timing of each unit active HSE was redistributed within the event (i.e. 'jittered') to generate a different matrix of population vectors that contained the same cells and rate within the event. We then established a distribution of replay scores by reconstructing from the same trial phase across 1000 shuffles. From this shuffled data we established a further score (replay score-z) showing the distance of replay score from the mean of the shuffled distribution by subtracting the mean of the shuffled data from the replay score and normalizing by its standard deviation (*35*).

Replay coherence score across brain regions

Once we had established significant replay events, we asked if these events were accompanied by sequences in the other brain region that followed this replay, or fired independently. To do so, we reconstructed a probability over position function for each window with spike data in the second brain region. This time we used the fit from the significant replay to calculate the score, which reflected the degree of coherent sequence activity. This replay coherence score was calculated by again summing probabilities within ± 4 bins from the line of best fit and dividing it by the number of windows (containing spikes) and expressed as a precentage. This score was compared to that produced from shuffled data (500 shuffles), which involved redistributing (i.e. jittering) the spike times derived from the second brain region within the event. With this

procedure we tested whether spiking in the second region took part in similar sequential firing and not merely the degree of spatial similarity between reconstructed locations in both brain regions. We generated a replay coherence z-score that reflected the distance of the spiking coherence to the shuffled data by first establishing the mean and standard deviation of the shuffled distribution. The replay coherence z-score (replay coherence z, Fig. S 13) represents the event replay coherence minus the mean of the shuffled data for that event, divided by its standard deviation.

We used a second form of shuffling in order to test whether the reconstructed trajectory matched the places encoded in the other, distal region better than any other places expressed during other trajectory replays (Fig S17). To produce a shuffled probability density function, we replaced each window containing no-zero probabilities with probabilities from other randomly selected windows taken from other significant replay events of the same trial type. Only time windows with non-zero probabilities were used to replace the original non-zero probabilities.

Drop analysis (within-region coherence score)

In order to validate our replay analysis and provide a comparison to the cross region replay coherence scores, we analyzed how 1, 2 or 3 cells within a given region followed replay exhibited within the same area. Taking those HSE's that exhibited significant replay with the full data set, we reestablished trajectories using the same rate maps, but this time dropping 1, 2 or 3 cells from the unit pool. Resultant trajectories that passed the criteria described above (i.e. maze coverage, replay speed and cell/spike number) were then used to generate within-region replay z scores with the dropped cells, as described above for the cross-region spike coherence. We performed this analysis for each cell, each possible pair of cells and 1500 randomly selected triplets of cells.

Local Field Potential (LFP) analysis

To identify periods of theta activity, the theta/delta power ratio was measured in 1600 ms segments (800 ms steps in between measurement windows), as previously described(*5*, *28*). Exploratory epochs included periods of locomotion or the presence of theta oscillations in the CA1 (as seen in the theta/delta ratio), including a < 2.4 s (i.e., two consecutive windows) transient from immobility segments. We then detected individual theta oscillations separately for each tetrode within both the CA1 and MEC, by filtering the LFP (5–28 Hz) during exploratory epochs and detecting the negative peaks of individual theta waves.

Theta phase modulation of significant replay was calculated by first selecting those events in which the peak of the HSE fell within a detected theta oscillation, recorded on a single sMEC electrode. The phase of the HSE was then calculated by performing a linear interpolation between the detected troughs of the cycle and calculating the mean angle, as previously described(*33*). The phase histogram in Fig. 2F represents the number of events in each phase bin (30º), divided by the total number of replay events (i.e., the probability of an event occurring during theta, at a given phase).

Ripple power during detected significant replay events was calculated using a channel from a single CA1 electrode with clear ripple oscillations, during sleep after exploration. For each event, we took a series of time points in 20 ms steps ± 500 ms from the peak of each HSE containing replay. Ripple power was then calculated in a 50ms window, centered on each 20 ms time step. The estimated ripple power in each step was normalized by calculating a z score, using the mean and SD of ripple power

established from the whole behavioral sessions (50ms windows, 50 ms steps).   This HSE ripple power profile was then averaged separately for sMEC and CA1 HSEs.

SWR detection was performed as previously described(*28*). Local field potentials were band-pass filtered (150–250 Hz), and a reference signal (from a channel that did not contain ripple oscillations) was subtracted to eliminate common-mode noise (such as muscle artefacts). The power (root mean square) of the filtered signal was calculated for each electrode and summed across electrodes designated as being in the CA1 pyramidal cell layer. The SWR detection threshold (7 SD above baseline) was always set in the first available sleep session, and the same threshold used throughout.

Cross-correlation analysis was performed to detect temporal alignment between significant replay and detected SWR, as well as between significant sMEC replay and CA1 HSEs. For the SWR analysis, HSEs with significant replay were taken as a reference and the number of detected SWRs was calculated in 25ms windows, centered on the peak of the HSE and extending to ± 500 ms. This was normalized by the total number of detected replay events.

Theta phase precession and theta sequence analysis

Individual place fields were detected by first detecting the position with the highest firing rate. A window was extended out from this peak until a bin was reached in which either the rate was greater than or equal to preceding bin. In order to avoid small fluctuation in the rate map, transitions that occurred above 70% of the peak rate were ignored. This process was then repeated iteratively on the remaining portions of the track until a peak of < 2 Hz was detected. Fields measuring narrower than 5 bins (14.67 cm) and with fewer than 50 spikes were disregarded from further analysis. In order to calculate a phase vs position correlation for each field we transformed the animal's position as a fraction of the length of the field.

The mean theta sequence was established with spikes that occurred during theta, but outside of any detected HSE. The trough of sMEC theta was used as a reference time point for both CA1 and sMEC analysis. Using the same algorithm described for the replay analysis, we generated a matrix of probability over position in 20 ms windows, with 10 ms steps between each window, up +-300 ms from each theta trough. For each set of position estimations, the positions were transformed from position to distance from the location of the animal as established at the time of the sMEC theta trough. The probabilities in each time window were normalized by the maximum probability, and the resulting matrices were then averaged across the whole recording. In order to calculated the slope of the session-mean theta sequence we used same the algorithm for trajectory fitting described in the replay analysis to establish the line of best fit within the averaged matrix. This was done iteratively in 100 ms windows in 10ms steps between -20 ms and +280ms, from which the steepest slope was selected. From this analysis we established the average slope for each region across days (Fig. S 10) as well as the maximal slope. In addition to calculating the mean theta sequence slope for a given session, we also detected theta sequences outside of HSE epochs. Having done so we could ask if the spiking in one region was coherent with theta sequences detected in the other and how coherence scores compared to that observed during waking replay. In order to detect theta sequences, we first generated windows from the peak-to-peak times of individual sMEC theta cycles, detected while the animal was actively engaged in the task (outside of the delay, moving at > 5cm/sec). Such windows that overlapped with a detected HSE or

contained fewer than 4 cells or 5 spikes were discarded from further analysis. Theta sequences were then reconstructed using the same algorithm described for the replay analysis, except that the reconstruction was only performed using the rate maps that related to the current trial type. The significance of the trajectory was then established using the place field rotation shuffling. To further ensure that the detected theta sequences did not represent undetected replay events, we selected the subset of trajectories with slopes <2 m/s and passed through or within 5cm of current location of the animal (CA1: N=2126, sMEC: n=665). Having established such theta sequences in both the sMEC and CA1, we then calculated the replay coherence scores for spiking in the other, distal brain region, using the same method described above.
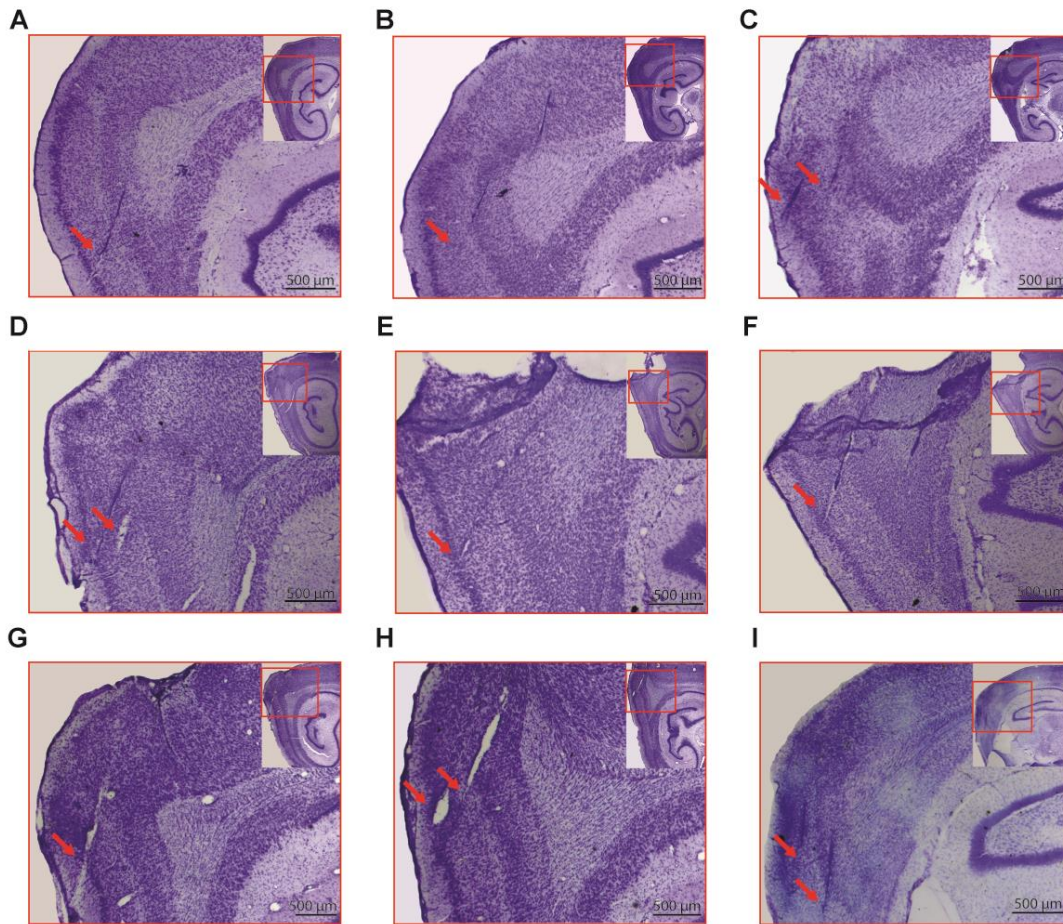
Fig. S1. Histological verification of electrode positioning

Sagittal Nissl-stained brain sections show electrode tracks terminating in the superficial layers of the medial entorhinal cortex for all rats. Inserts show the entire region; red boxes delineate the magnified region; red arrows indicate tracks in the area of interest, **(A–C)** rat 1, **(D–F)** rat 2, **(G–H)** rat 3, **(I)** rat 4 (correspond to units shown in Fig.1).
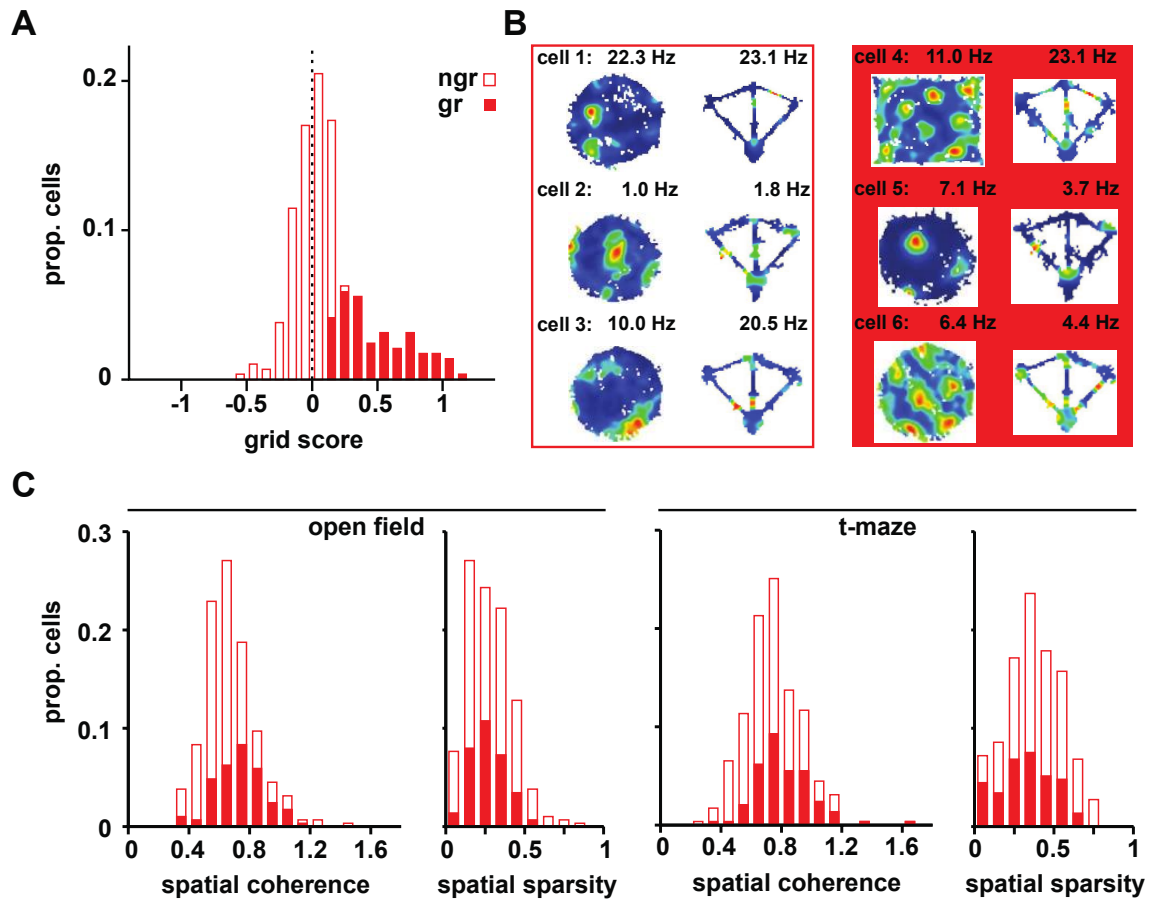
Fig. S2. Grid cell characterization

(**A**) Distribution of grid scores within the recorded superficial layers of the medial entorhinal cortex (sMEC) population. Red solid bars mark cells with a grid score greater than the 95 percentile of the shuffle distribution. See methods, n=91 grid cells (gr) and 204 non-grid cells (ngr).

(**B**) Examples rate maps established in the open field and T-maze of non-grid (left panel, red outline) and grid cells (right panel, solid red).

(**C,D**) Spatial characteristics of grid and non-grid cells. Rate map coherence(*32*) (left) and sparsity(*33*) (right) are shown for the sMEC population in the open field (left panel) and T-maze (right panel).
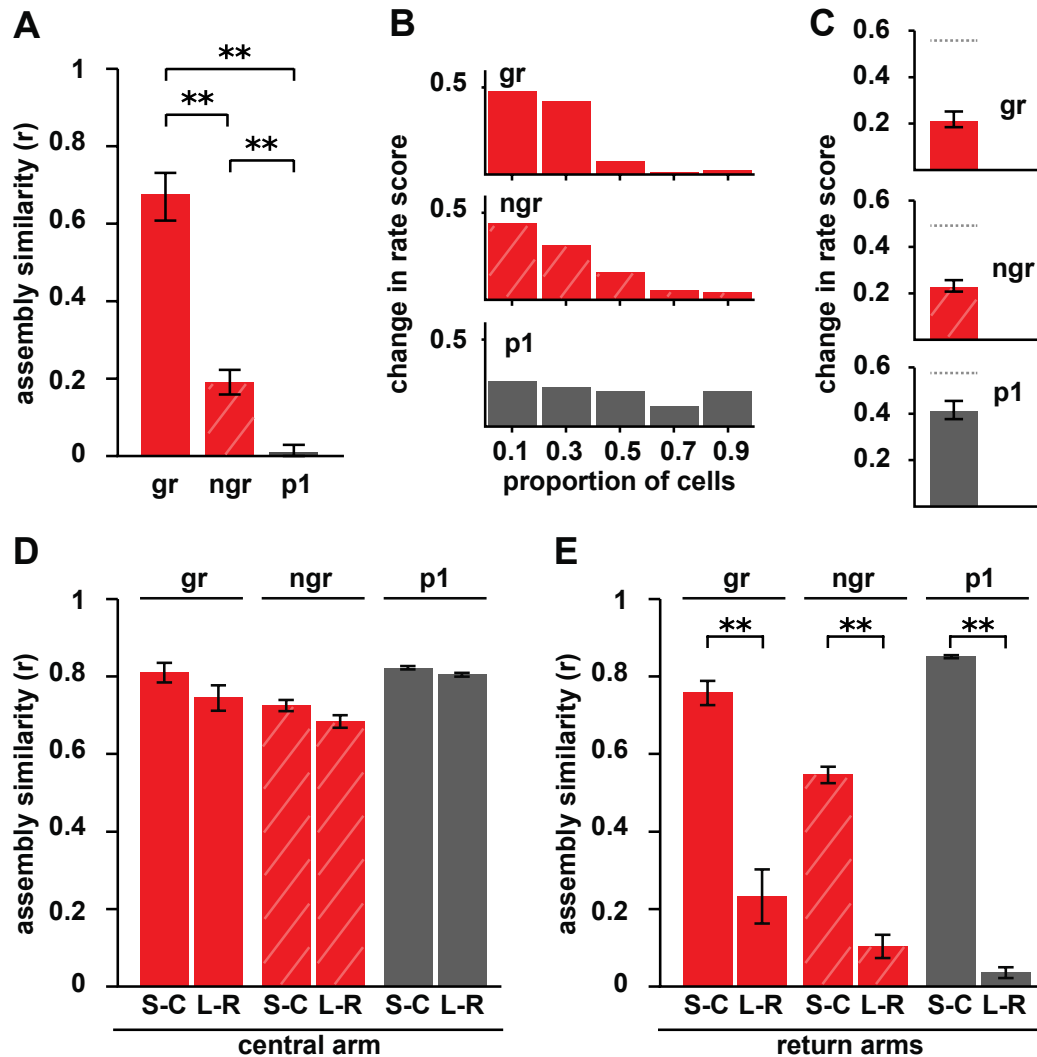
Fig. S3. Reorganization of sMEC and CA1 region spatial firing patterns between environments and trial phases

(A) Reorganization of spatial assembly patterns between the open field and the T-maze. Assembly similarity compares the similarity between place-rate maps for pairs of cells in the open field to that in the T-maze (see methods). A high correlation indicates that cells with overlapping place fields in one environment are similarly overlapping in the second, and vice versa. Solid red bars, gr: sMEC grid cells (n=304 cell pairs); striped red bars, ngr: sMEC non-grid cells; dark grey bars, p1: CA1 region pyramidal cells. Error bars: 95% confidence intervals. ** p<0.00001, z-test(*31*). Note that the grid cell population shows a similar configuration of rate maps between the two environments, in contrast to non-grid cells and CA1 pyramidal cells.

(B,C) Reorganization of spatial firing rates. We measured the peak firing rate within each rate map (i.e. from the bin in the rate map with the highest firing rate) in both the T-maze and the open field and generated a normalized change in rate score (absolute value of the difference/sum), for each cell(*24*). Cells with a peak rate of less than 1 Hz in both environments were excluded (gr n=84, ngr: n=195, p1: n=375). The distribution of these scores is shown for each population of cells in (B) as well as the median in (C). Error

bars in (C): 95% bootstrapped confidence interval. Color code and abbreviations as in (A). Grey dotted line: the chance level, generated from shuffled data (see methods). Note that all three cell types show a weaker than chance spatial firing rate reorganization.

(D,E) Reorganization of spatial assembly patterns between different trial phases on the T-maze.We used the assembly similarity score (described in (A) and methods) to compare changes in spatial coding across different trial phases (sample vs. choice: S-C and left vs. right: L-R). On the central arm (D, see blue highlighted region on figure 1), spatial assemblies were highly correlated between all phases (all r>0.5), regardless of cell type. Between the goal and the end of the track (E, return arms), sample and choice trials were significantly more correlated, than when comparing assembly organization between the left and right arms. Error bars: 95% confidence intervals(31). All **p<0.00001, z-test (*24*). Color code and abbreviations as in (A).
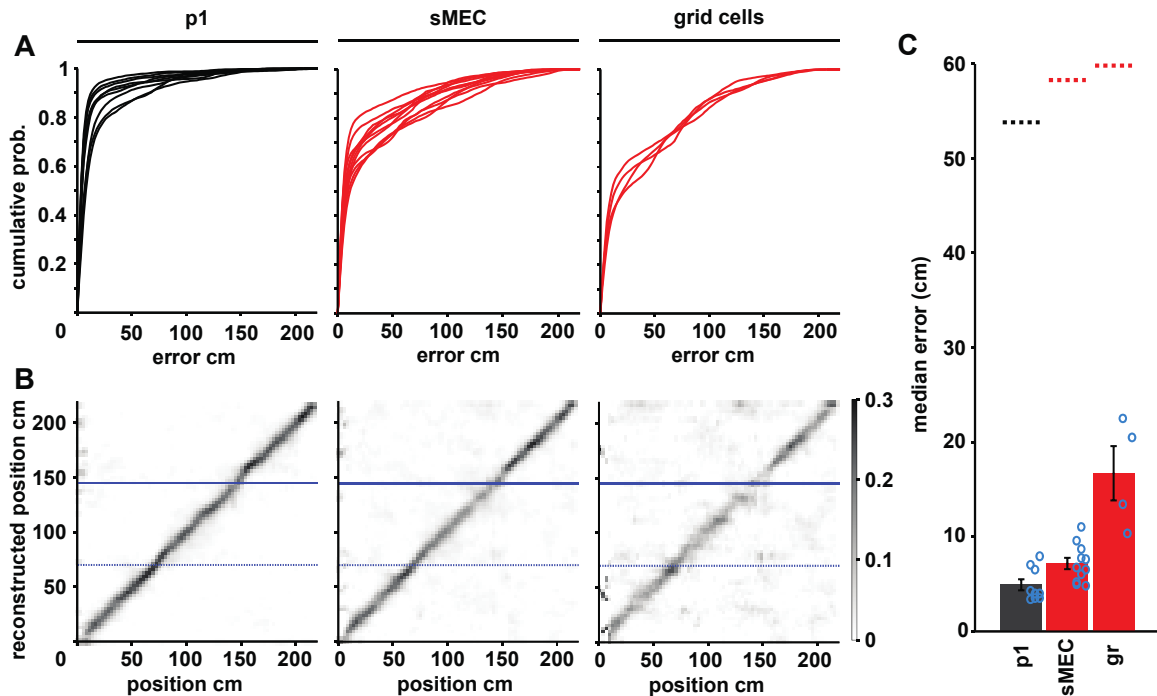
Fig. S4. Position reconstruction during exploration

We used a Bayesian maximum likelihood method to reconstruct the position of the animal using previously established rate maps and instantaneous firing patterns as the animal performed the task (see methods). In order to quantify the accuracy of the position decoding, we employed a cross validation approach by constructing rate maps from all trials except from the one in which the error was measured. We repeated the same procedure for each trial to measure the mean error. Instantaneous firing rates measured in 500 ms windows (250 ms overlap, see methods).

(A) For each cell type we show the session-by-session cumulative errors. Note the high probability of reconstructing a similar position to which the animal was currently occupying, in all cases. Left panel, black: CA1 pyramidal cells (p1): n=9 sessions with an average of 45.56 cells (range: 27-63 cells). Middle panel, red: all sMEC: n=11 sessions, with an average of 24.6 cells (range: 19-44 cells). One session with <19 cells was excluded. Right panel, red: grid-cell only: n=4 sessions with at least 10 cells (10, 11, 12 and 12 cells, respectively).

(B) Example confusion matrices for all CA1 (left), all sMEC (middle) and grid cell only (right) reconstruction, using data gathered from a single animal.

(C) The median error is shown for the different cell types (p1, black: CA1 pyramidal cells; sMEC, red: all sMEC cells; gr, red: grid cells only). Circles show the median error for each session. Error bars: SEM.

15
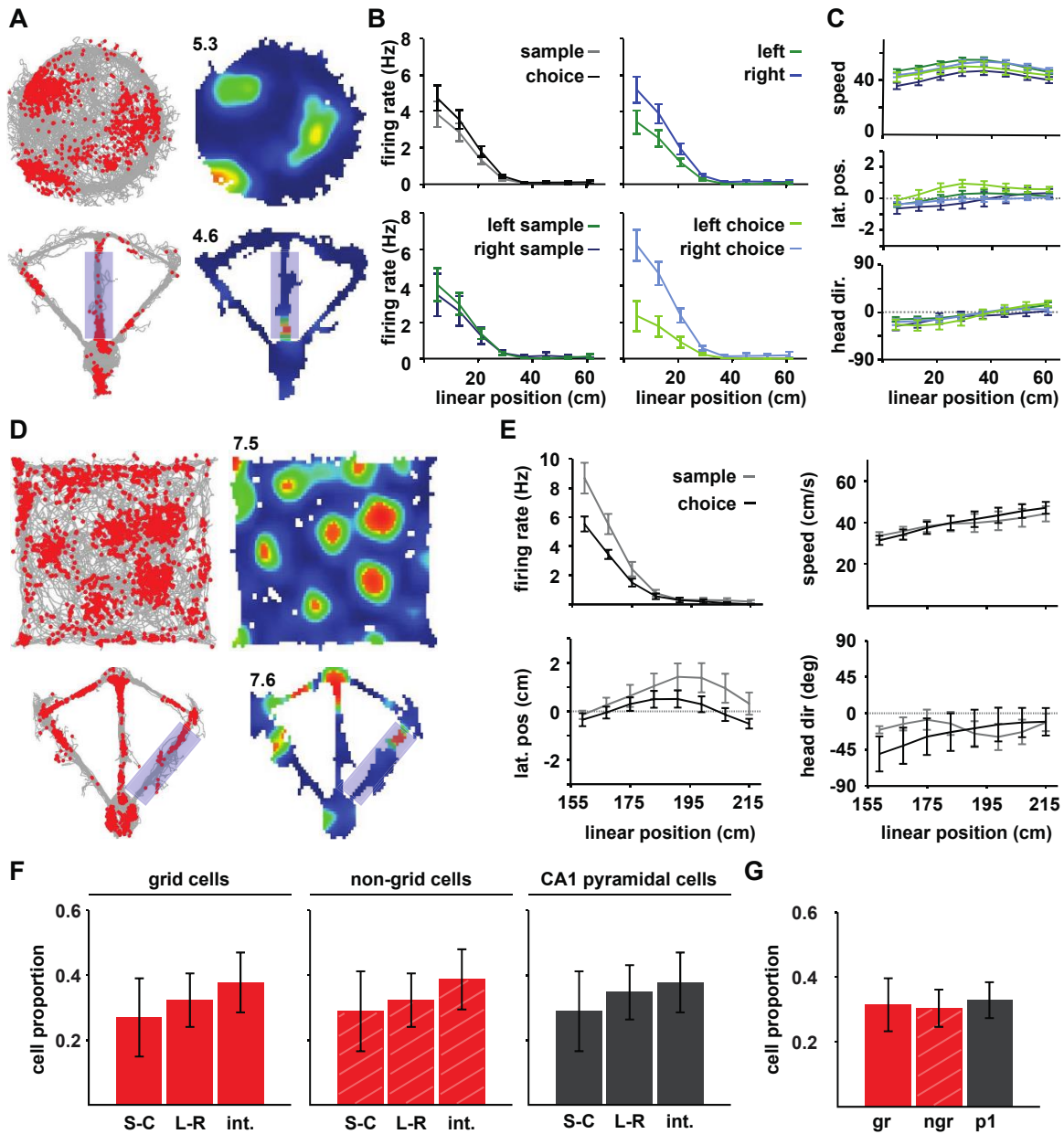
Fig. S5. Change in firing rate with trial phase

(A-C) Example of a grid cell that shows elevated firing rate on right trials with an interaction with forced and choice (p<0.005, Ancova, see methods). (A) Spike position overlaid on tracking data (left) and rate maps (right) are shown for open field exploration (top) and T-maze task (bottom). Peak firing rate (top left of the rate map) in Hz. The start track is highlighted in blue. (B) Linearized rate maps (8cm bins) were calculated trial-by-trial and averaged by trial phases. Top left: sample (grey) vs. choice (black); top right: left (green) vs. right (blue); bottom left: left sample (dark green) vs. right sample (dark blue); bottom right: left choice (light green) vs. right choice (light blue). (C) Along with rate presented in (B), we simultaneously calculated speed (top), lateral position (i.e. distance from the center of the track to the edge, $\pm$ 5cm, middle) and head direction (bottom) in each spatial bin. Head direction exceeding $> \pm 90^\circ$ from the direction of travel

were excluded from further analysis. Speed, lateral position (lat. pos.) and head direction (head dir.) are plotted as a function of linear position for different trial phases. Color code as in (B). Error bars: SEM.

(D,E) Example of a grid cell exhibiting sample/choice rate modulation on the return arm (i.e. between goal and the delay area, highlighted blue, $p<0.001$, Ancova). Spike position and rate maps are shown (D) along with linearized rate maps and behavioral quantification (E). Layout, color code and abbreviations as in (A, B).

(F,G) Percentage of cells that show significant rate modulation on the central track (F) and between the goal and the return arm (G). (F) Left, red: grid cells only; middle, red stripped: non-grid cells; right, dark grey: CA1 pyramidal cells. S-C: sample vs. choice, L-R: left vs. right, int: interaction. Error bars: C.I. 95%. (G) gr: grid cells, ngr: non-grid sMEC. p1: CA1 pyramidal cells. Color code and error bars as in (F).
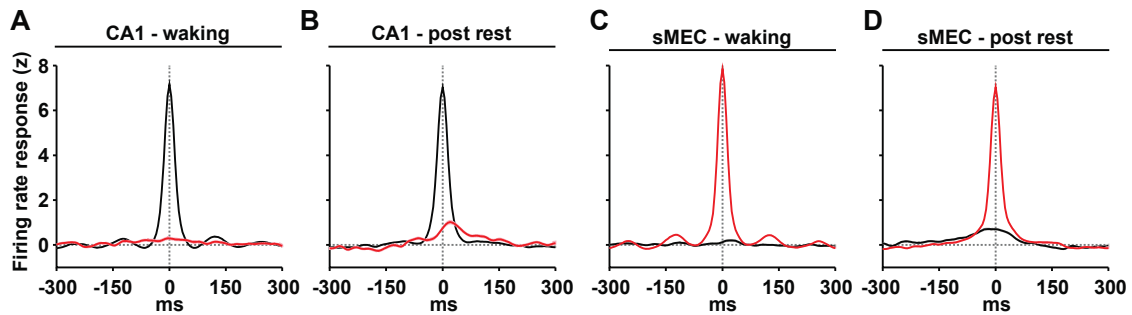
Fig. S6. Firing response during HSE

　　(A,B) Firing response of CA1 (n=410, black line) and sMEC (n=295, red line) cells to the CA1 HSEs detected in waking (A, CA1 - waking) and in sleep (B, CA1 - post rest). We performed a cross-correlation (5 ms bins) to the HSE peak. For each cell, firing rate in the cross-correlation was transformed into a z-score by calculating the mean rate across all bins and dividing by the standard deviation. The resulting histogram was smoothed with a Gaussian kernel (sd=5 ms) and averaged across the population of cells.

　　(C,D) We performed the same analysis as in (A) and (B) with sMEC HSEs. Similarly, CA1 showed little response during waking, while showing a weak increase during rest HSEs. Layout, color code and abbreviations as in (A, B).
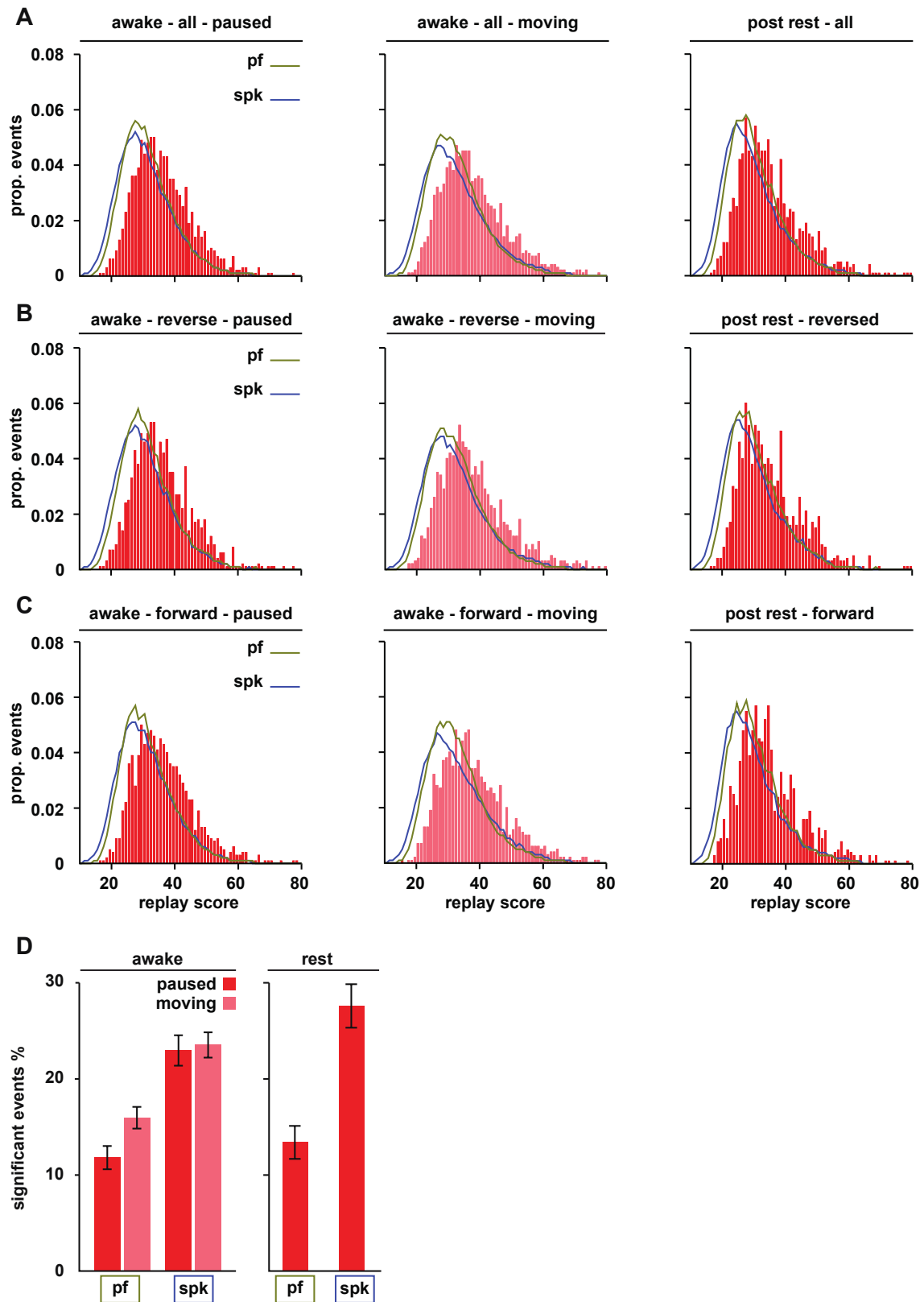
Fig. S7. SMEC replay across all behavioral epochs

Distribution sMEC replay scores are shown for different behavioral epochs, along with shuffled distributions (place field shift, pf: green and spike jitter, spk: blue, see methods).

(A) We identified a total of 2178 high synchrony events (HSE) during periods when the animal paused (<5 cm/s, awake - all - paused, red), 4024 sMEC HSE's during active locomotion (>=5 cm/s, awake - all - moving, light red) and 1506 during rest (post rest – all, red). The distribution of replay scores was significantly different from shuffled data in all behavioral epochs, regardless of the type of shuffling (all $p<10^{-27}$, KS test).

(B,C) As in A, sMEC HSE's with reverse (B: paused n=1381, moving n=1977 and sleep n=756) and forward (C: paused n=1337, moving n=2027 and rest n=749) trajectories, which had significantly different distributions to that of both sets of shuffled data (all $p<10^{-27}$, KS test). Layout, color code and abbreviations as in (A).

(D) Proportion of HSE's showing significant replay, during waking (left) and rest (right). When considering place field shuffling (pf), we detected 321, 642 and 202 events with a score larger than the 95 percentile during pauses, movement or rest respectively. With spike jitter shuffling (spk), 624, 947 and 416 events showed significance for the same epochs. Left panel: red bars: awake - all - paused; light red bars: awake - all - moving.
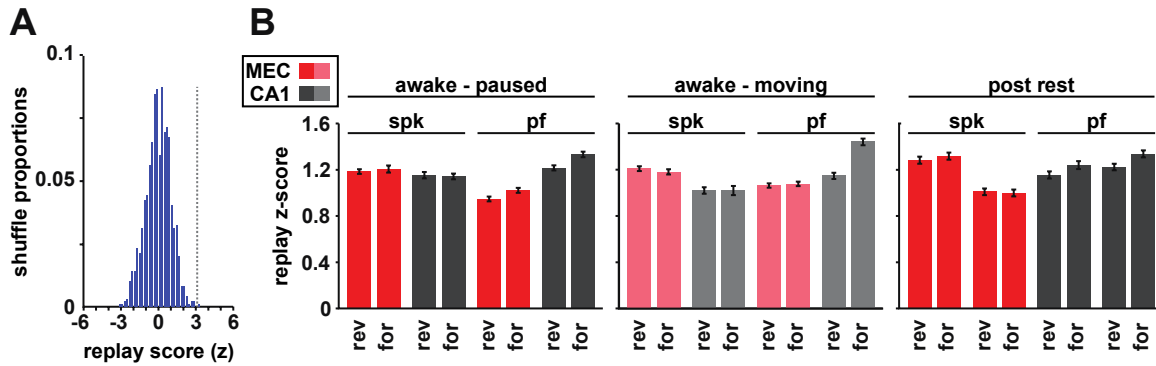
Fig. S8. Z-score of replay scores for forward and reverse replay

We established a replay z-score for each event, to provide a measure of how each event related to the shuffled distribution (replay z-score, see methods). For each HSE we calculated the mean and standard deviation of the shuffled distribution and used these values to normalize each replay score. **(A)** Example. Dotted line: replay score for a single event **(B)** Reverse (rev) and forward (for) CA1 (grey) and sMEC (red) replay at all behavioral epochs more often exhibited positive z-scores than expected by chance, regardless of the shuffling method used (all $p<10^{-16}$, binomial test). Left: awake - paused; middle: awake - moving, lighter colors; right: post rest. spk: spike jitter shuffling; pf: place field shuffling. Error bars: SEM.
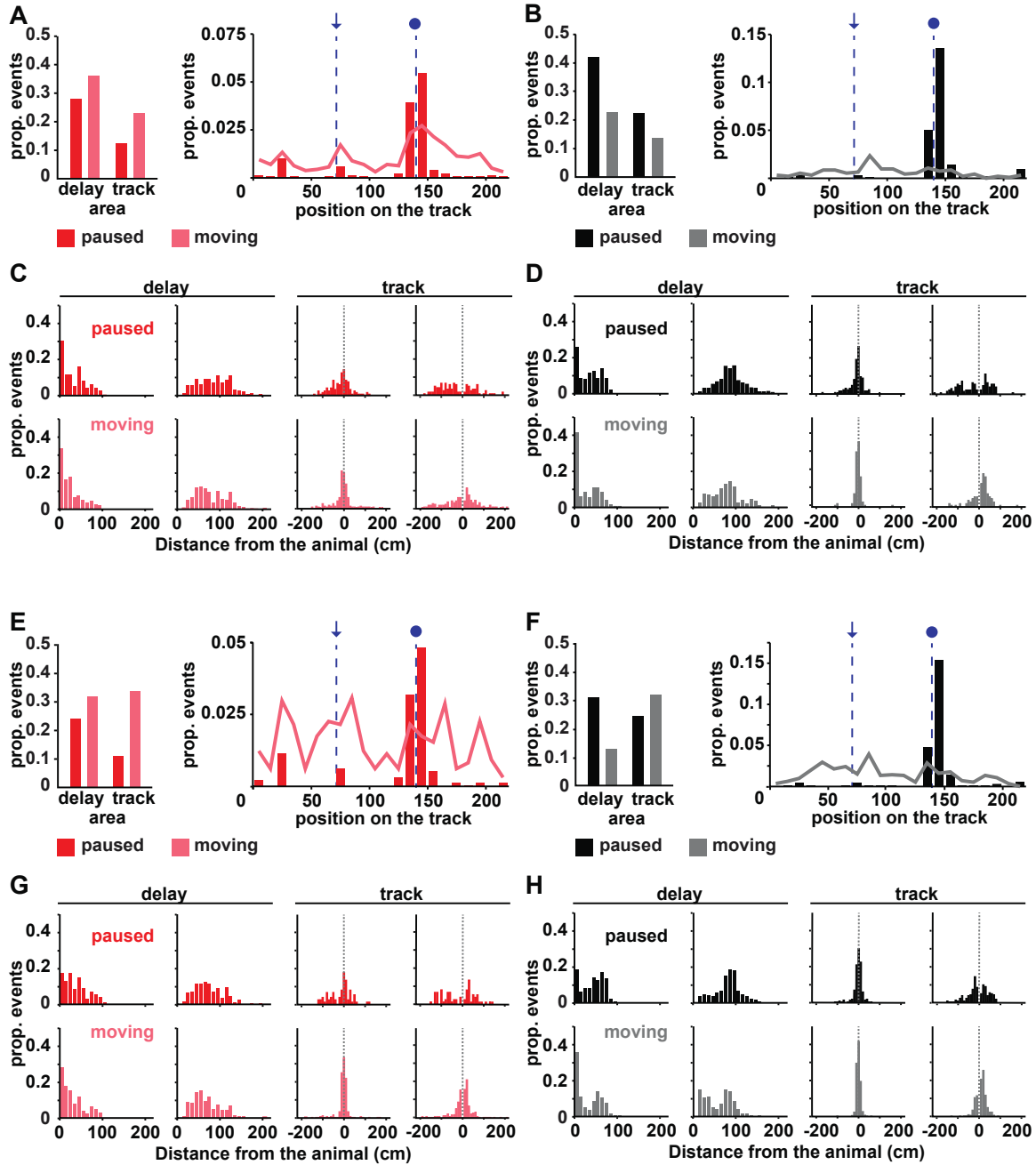
Fig. S9. Waking replay in the sMEC and the CA1

(**A,B**) Distribution of HSE's containing significant sequences generated in the sMEC (A) and CA1 (B), selected using spike order jitter shuffling (see methods). Left panels show the proportion of events detected while the animal had either paused (< 5 cm/s; (A) sMEC, red; (B) CA1, black) or was actively engaged in locomotion (>= 5 cm/s; moving; (A) sMEC, pink; (B) CA1, grey), for delay epochs (delay area) and during the task itself (track area). Right panels show the locations of events during the task itself. Arrow indicates the choice point, while circle marks the goal. Color code as in left panel.

(**C,D**) sMEC (C) and CA1 (D) waking replay often encodes locations related to the current position of the animal, as well as non-local positions. Shown is the distribution of

distances from the closest point (left) and furthest point of replay (middle left) that occurred during delay epochs, as well as on the track (closest point: middle right, furthest point: right). Only replay trajectories reflecting the same left-right turn are included in the analysis (sMEC paused: 45.7%, moving 50.8%, CA1 paused 54.13%, moving 69.1%). Top row: replay that occurred while the animal had paused (< 5cm/s, dark colors). Bottom row: replay detected when the animal was moving ($\geq$5cm/s, light colors). Color code as in (A,B).

(E–H) Shows the same analysis for events detected with place field shift shuffling. On the track 53.8% and 63.67% of sMEC replay trajectories represented the same left-right turn for when the animal paused, or was moving respectively. In the CA1, 65.1% of trajectories during pauses represent the same side as that occupied by the animal, and 77% while the animal was moving.
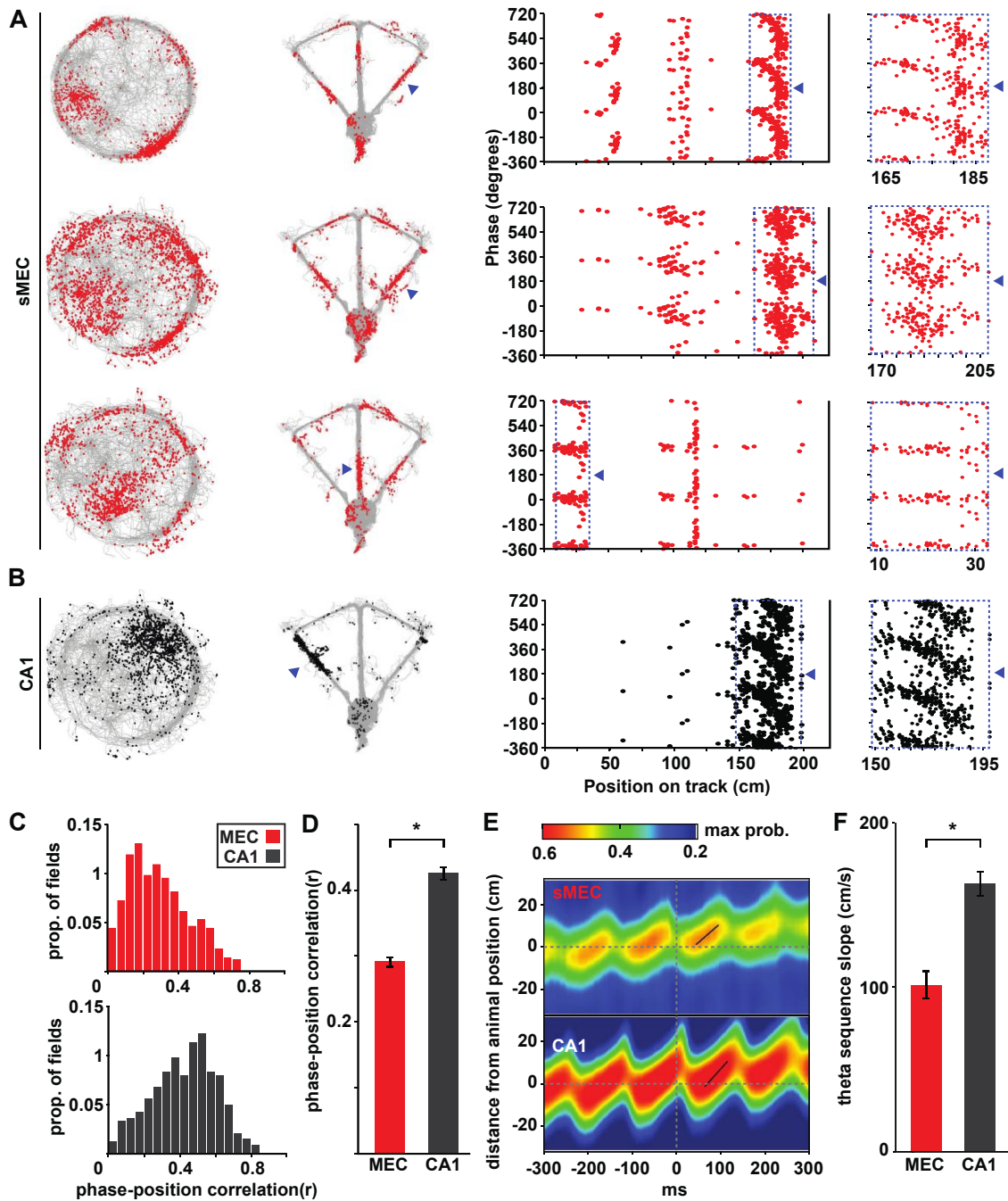
Fig. S10. Phase precession and theta sequences in CA1 and the sMEC

In the CA1 theta phase precession is known to give rise to the generation of spiking sequences that encode a series of positions, extending from behind to the front of the current location of the animal, within a single theta cycle(*33*). It has been shown that subsets of excitatory cells in the sMEC also phase precess(*38*), which may in turn be detected as sMEC replay during exploratory epochs. To examine this possibility we established the degree of theta phase-position coding within our population of sMEC

cells, and the slope of the theta sequence that it may give rise to. Color code throughout: sMEC red, CA1 black.

(A,B) Examples of the relationship between spike theta phase and position in three sMEC units (A) and a single CA1 unit (B). Left panels show the animal's path and position of the spikes during open field exploration (furthest left) and running on the T-maze (middle left). The middle right panel shows the phase and linear position of each spike, for a single arm of the T-maze. Blue doted box highlights the place field indicated by the blue arrow on the middle left panel. Right panel is a zoom in of the section of the track containing the place field highlighted in the middle right panel.

 (C) Distribution of circular linear correlations for individual place fields detected from the sMEC population (n=570) and CA1 region pyramidal cells (n=337, see methods). **(D)** Comparison of the means of the distributions presented in (C) showing that such theta phase precession is significantly weaker in the sMEC units than for CA1.

(E) Typical example of a mean theta sequence probability map and slope (see methods), established from a single recording day for the sMEC (top) and CA1 (bottom) populations. Position reconstruction is shown as a function the animal location in 10 ms steps +-300 ms from the trough of each theta cycle detected in the sMEC. Black line denotes the fit with the steepest slope within -20 ms and +280ms of the theta trough.

(F) Across recording days, the mean slope was significantly weaker in the sMEC than in CA1.
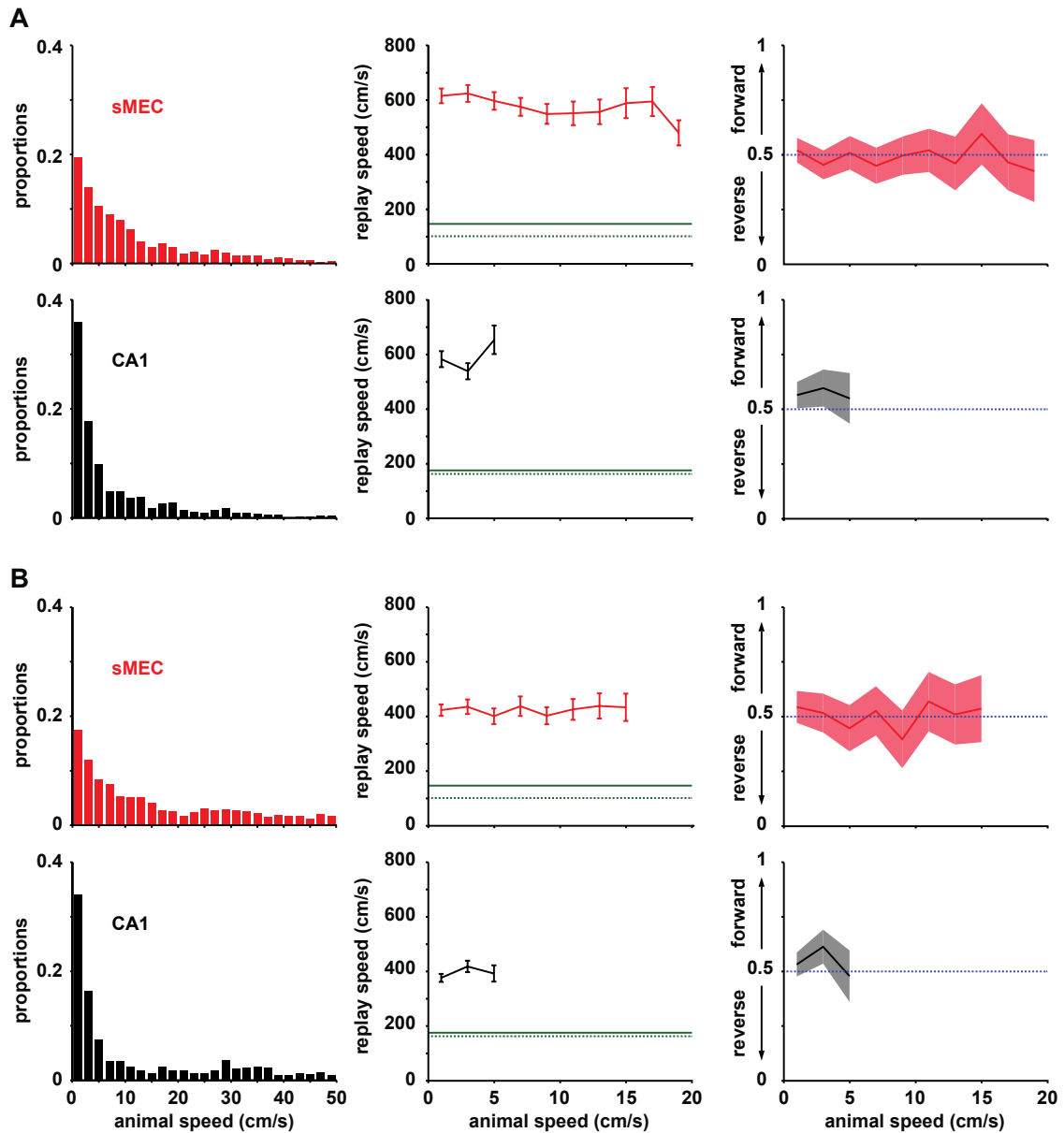
* p< 0.01, Kruskal Wallis test.

Fig. S11. Characterization of waking replay sequences

(A,B) Analysis of all replay events detected during waking HSE's that showed a better replay score than that from either the spike order shuffling (A) or place field shuffling (B), including those that were below the replay slope threshold of 200 cm/s (spike order shuffling: sMEC n=1790, CA1 n=1042; place field shuffling: sMEC n=1183, CA1 n=1337). Throughout: top row sMEC (red), bottom row CA1 (black). The left panels show the proportion of significant events detected at different animal speeds. The middle panels show the mean replay speed (slope of the fitted replay trajectory), for different animal speeds. Bins with < 40 events were not included in the plot. Error bars SEM. Green dotted line: average mean theta sequence slope as shown in Fig. S9 (D). Solid green line: steepest mean-theta sequence slope across all sessions. Note that the mean replay speed is 2-3 fold faster than that seen from the mean-theta sequence

analysis, for both the CA1 and sMEC. The right panels show the proportion of forward and reverse replay, for different animal speeds. Shaded region: 95% confidence intervals. Note that replay sequences in the sMEC continue to exhibit reverse replay, even when the animal is moving at faster velocities.
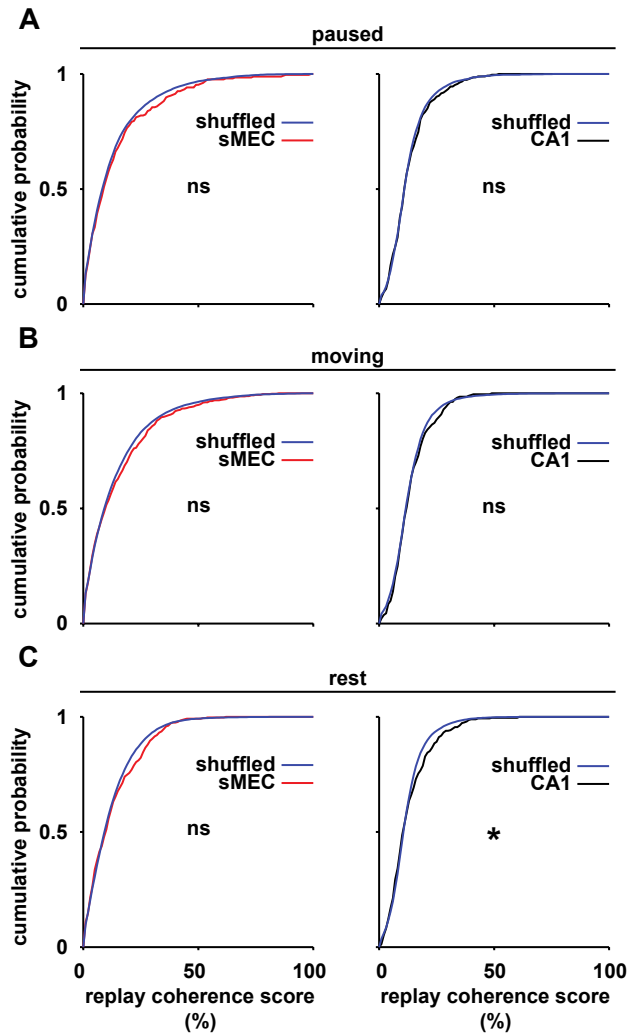
Fig. S12. Replay coherence between regions when replay trajectories were identified with order shuffling

HSE's with significant replay were selected by order shuffling in both the sMEC (left panel, red lines), and the CA1 (right panel, black lines). Cumulative distributions are shown for replay coherence between detected sequences and spiking in the other brain area, along with the shuffled distribution (blue lines) for different behavioral epochs. **(A)** Waking immobility (< 5cm/s, paused, sMEC n=255, CA1 n=273). **(B)** Active locomotion (>= 5cm/s, moving, sMEC n=597, CA1 n=275). **(C)** Rest (sMEC n=366, CA1 n=296).

Replay coherence was not significantly different from the shuffled distribution (all p>0.1, KS test) when either considering sMEC replay with CA1 unit activity, or CA1 replay with sMEC unit activity, except for post-rest epochs, where CA1 sequences show a significant relationship with sMEC unit activity (C, right panel p=0.038, KS test).
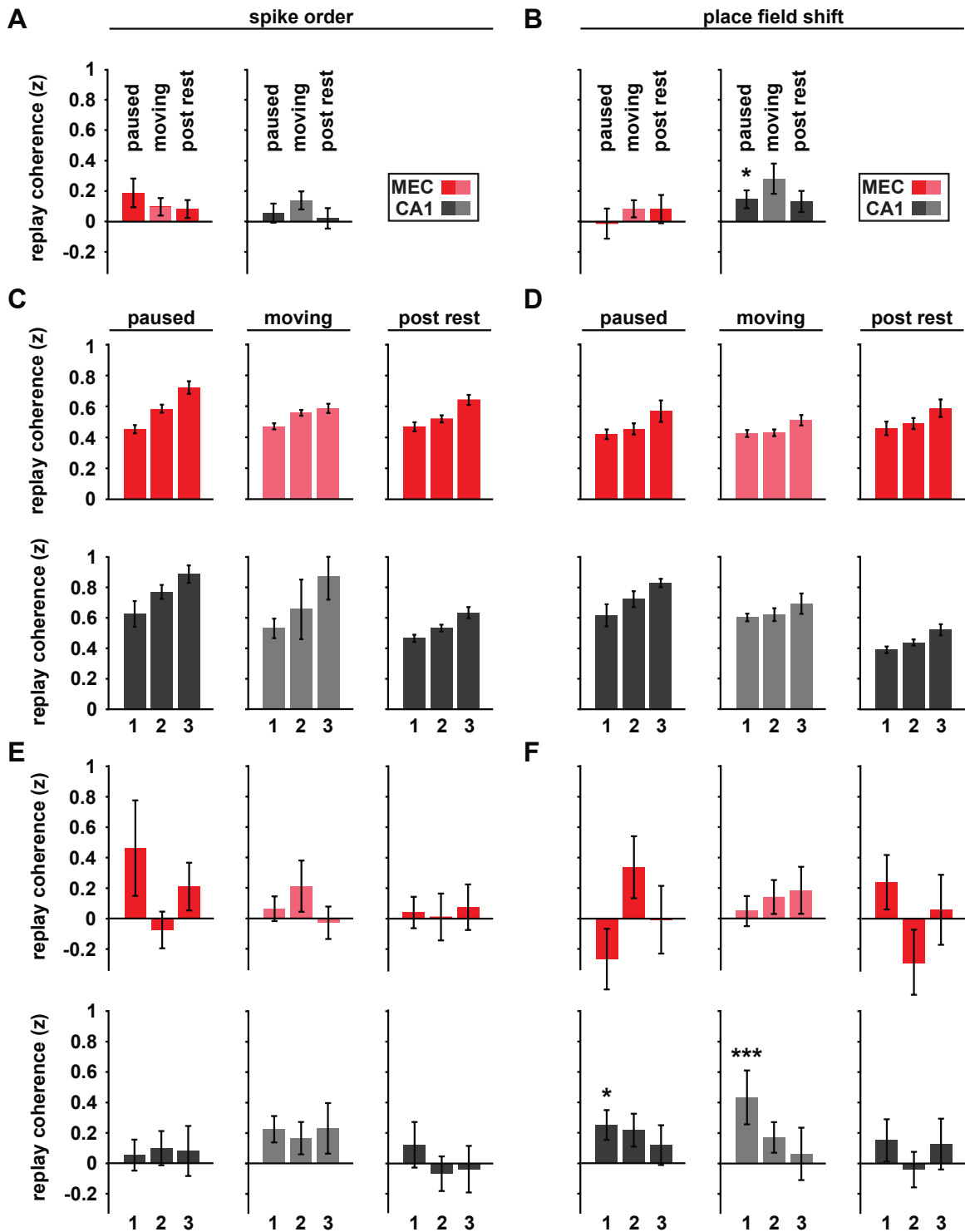
Fig. S13. Replay coherence within a region is stronger that between the sMEC and CA1 areas

(A,B) Replay coherence z-scores (see methods) between significant sMEC and CA1 ensemble firing patterns (left panel, red) and between CA1 sequences and sMEC activity (right panel, grey) for different behavioral epochs: waking immobility (< 5cm/s, paused);

active locomotion (>= 5cm/s, moving, lighter colors); rest (post rest). **(A)** Sequences detected with spike order shuffling (paused: sMEC n=255, CA1 n=273; moving: sMEC n=597, CA1 n=275; rest: sMEC n=366, CA1 n=296). **(B)** Place field shift shuffling (paused: sMEC n=115, CA1 n=295, moving: sMEC n=412, CA1 n=363; post rest: sMEC n=173, CA1 n=293). *p<0.05, more events than expected by chance greater than 0, binomial test.

   (C,D) Within region sequence coherence based on spike order shuffling (C) or place field shift shuffling (D). In order to validate our replay event detection, we first dropped 1, 2 or 3 cells from the sMEC (top panels, red) or the CA1 (bottom panels, grey) population and detected trajectories using the remaining population of units. These new trajectories allowed us to calculate coherence scores with the dropped cells (see methods). Significant trajectories were identified with the shuffling. Dropped cells showed sequence coherence z-scores that were significantly different from 0, in all cases. (p<0.000001, binomial test). Color code as in (A,B).

   (E,F) Cross-region sequence coherence analysis based on spike order shuffling (E) or place field shift shuffling (F). We calculated for each significant sMEC and CA1 sequence the replay coherence z-scores for sequences in which 1, 2 or 3 units were active in the other brain region. Note that sequence coherence z-scores were weak in all cases, with few showing a coherence z-score significant (*p<0.05, ***p<0.0005 binomial test). Error bars: SEM. Color code as in (A,B).
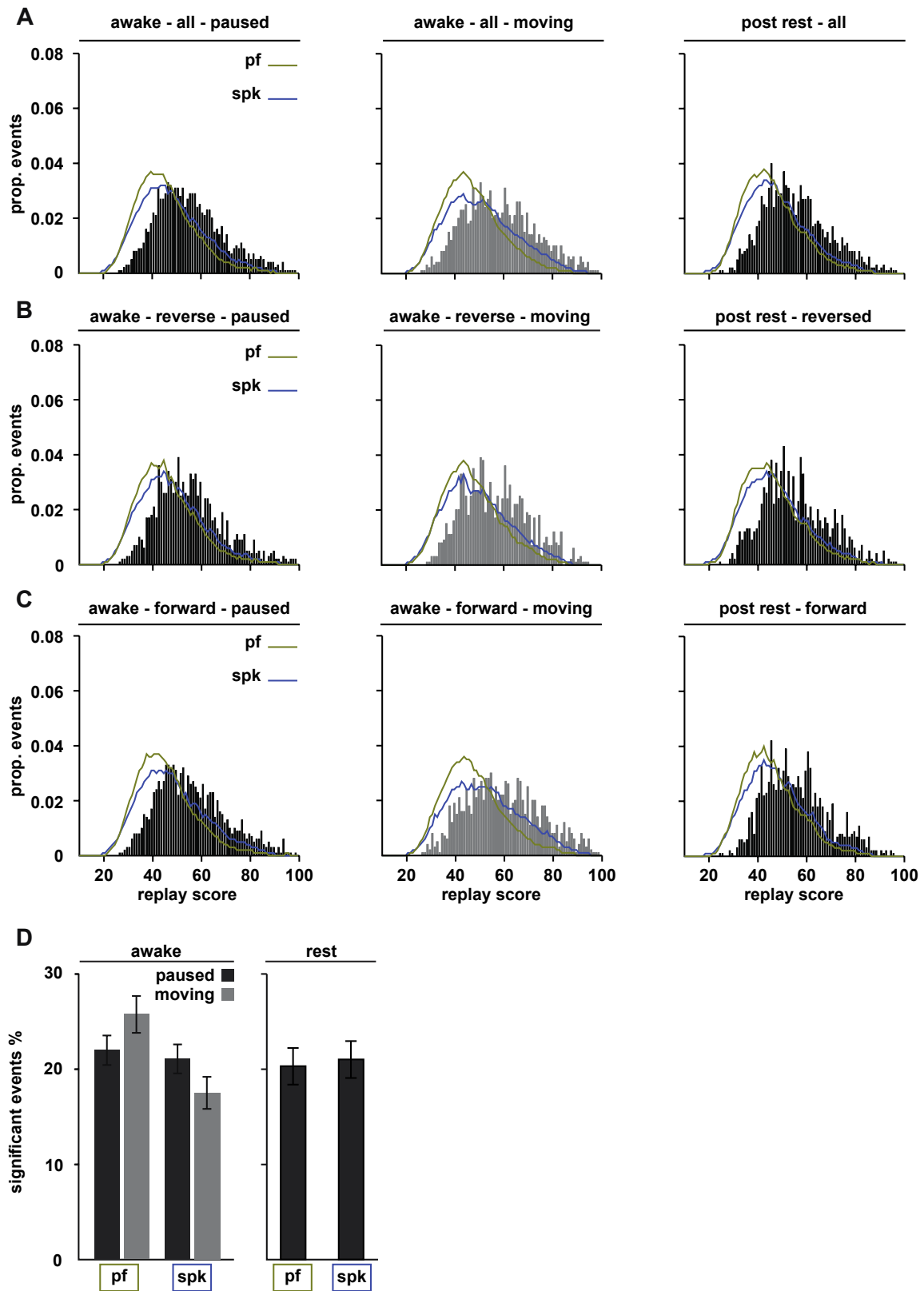
Fig. S14. CA1 replay across all behavioral epochs

Distribution CA1 replay scores are shown for different behavioral epochs, along with shuffled distributions (place field shift, pf: green; spike jitter, spk: blue, see methods).

(A) We identified a total of 2750 HSE's during periods when the animal paused (<5 cm/s, awake - all - paused, black), 1958 CA1 HSE's during active locomotion ($\geq$5 cm/s, awake - all - moving, grey) and 1693 during post-rest (post rest - all, black). The distribution of replay scores was significantly different from shuffled data in all behavioral epochs, regardless of the type of shuffling (all $p<10^{-44}$, KS test).

(B,C) As in A, CA1 HSE's with reverse (B, paused n=1317, moving n=892 and sleep n=817) and forward (C, paused n=1433, moving n=1066 and rest n=876) trajectories had significantly different distributions to that of both sets of shuffled data (KS, all $p<10^{-44}$). Layout, color code and abbreviations as in (A).

(D) Proportion of HSE's showing significant replay, during waking (left) and rest (right). When considering place field shuffling (pf), we detected 605, 503 and 344 events with a score larger than the 95 percentile during pauses, movement or rest respectively. With spike jitter shuffling (spk), 580, 343 and 356 events showed significance for the same epochs. Left panel: dark grey bars: awake - all - paused; light grey bars: awake - all - moving.
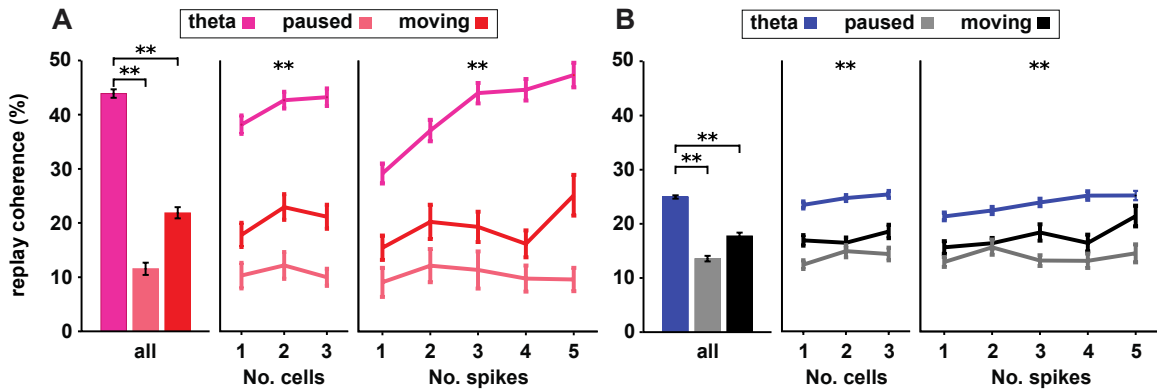
Fig. S15 Replay coherence during theta oscillations

Trajectory sequences were reconstructed during peak-to-peak theta oscillatory cycles taking only events with a minimum of 4 cells and 5 spikes, as well as trajectory slopes of <2m/s (see methods). The coherence of sMEC theta trajectories to CA1 activity (**A**) and CA1 trajectories to sMEC (**B**) were measured. For comparison, the coherence for theta oscillation-related trajectories (theta) are displayed with equivalent replayed trajectories during waking immobility (<5cm/s, paused) and active locomotion (≥5cm/s, moving). The left panels show that average replay coherence while the middle and right panels display the mean of events with a different number of cells or spikes that were present in the distant region, i.e., activity for CA1 (**A**) and sMEC (**B**). The coherence for trajectories during theta sequences were always significantly higher than that to replayed trajectories (all $p<10^{-15}$, Anova). Error bars: SEM.
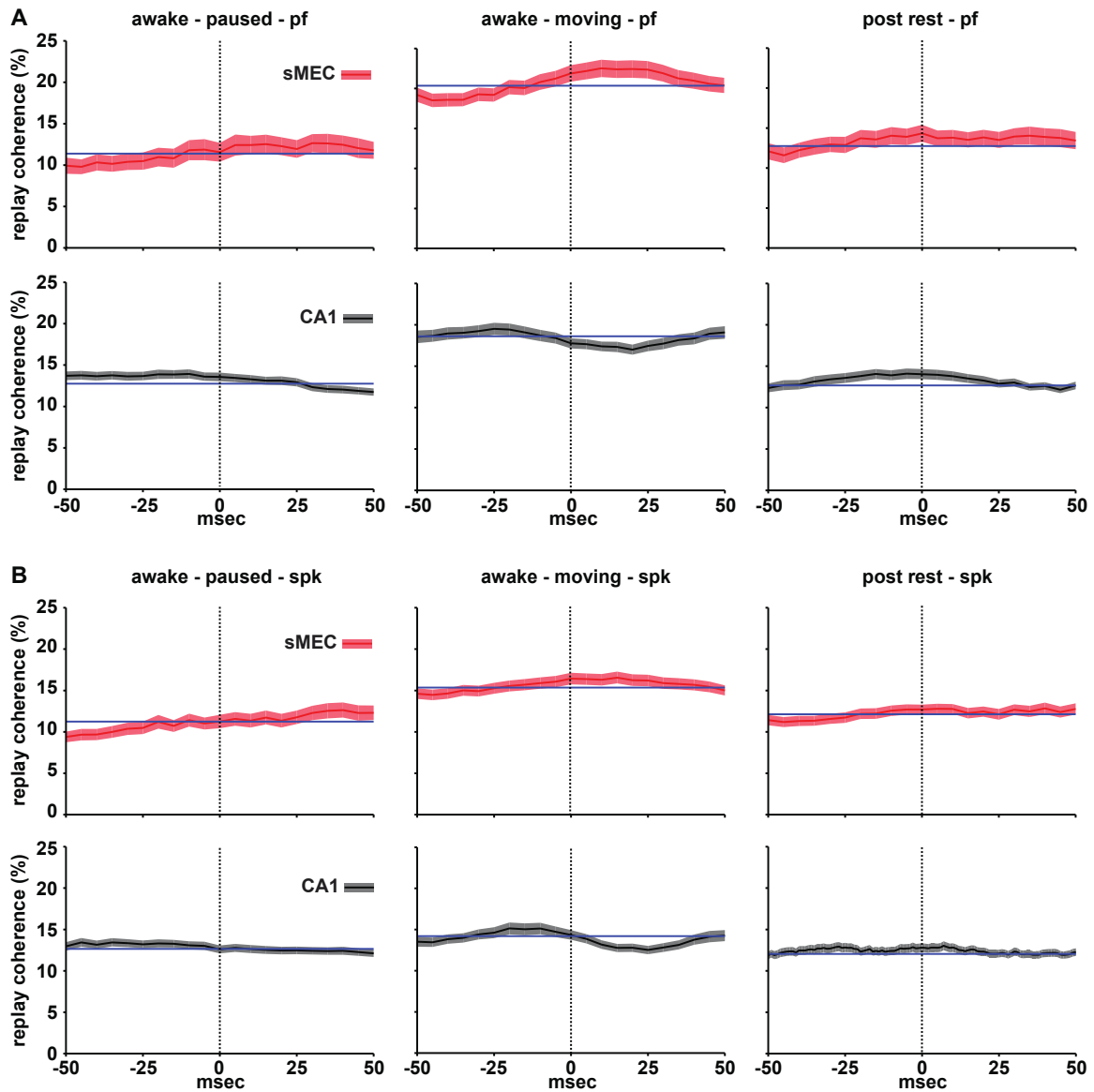
Fig. S16. Replay coherence at different time lags

(A,B) Significant sMEC (top row, red) and CA1 (bottom row, black) replay events were selected by either place field shift (A, pf) or spike jitter shuffling (B, spk) for different behavioral epochs: waking immobility (< 5cm/s, awake - paused, left panel); active locomotion (>= 5cm/s, awake – moving. middle panel); rest (post rest, right panel). Replay coherence scores were calculated between significant events and spiking in the other brain region, at lags of ±50 ms, in steps of 5ms. No significant change in score could be seen with time lag (all $p > 0.08$, anova Tukey HSD). Blue line: mean across all time windows. Shaded regions: SEM.
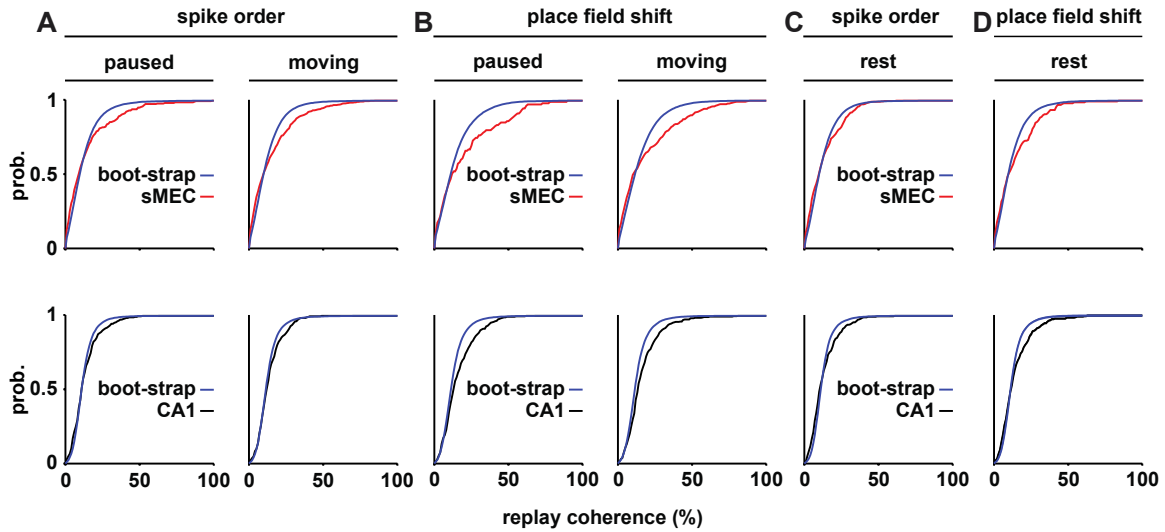
Fig. S17 Replay coherence between regions: checking for nonaligned matches between trajectory in one region and the expressed place in the other region

HSE's with significant replay were selected by order shuffling **(A,C)** or place field rotation **(B,D)** in both the sMEC (top panels, red lines), and the CA1 (bottom panels, black lines). For the shuffled distributions, the Bayesian probability distributions of the distant brain area were randomly selected from other significant replay events (see methods). Cumulative distributions are shown for replay coherence between detected sequences and spiking activity in the other, distant brain area, along with the place-randomized shuffled distribution (blue lines) for different behavioral epochs. **(A,B)** Replay during waking immobility (< 5cm/s, paused) and active locomotion (≥ 5cm/s, moving). **(C,D)** Replay during rest. Replay coherence was significantly different from the shuffled distribution (all p<0.05, KS test).